
Leeward Flow Over Delta Wings at Supersonic Speeds

Joachim G. Szodruch and David J. Peake

April 1980



National Aeronautics and
Space Administration

NTT 8-2703

U.S. GOVERNMENT PRINTING OFFICE
WASHINGTON, D.C. 20540

3 1176 00188 3926

Leeward Flow Over Delta Wings at Supersonic Speeds

Joachim G. Szodruch

David J. Peake, Ames Research Center, Moffett Field, California



National Aeronautics and
Space Administration

Ames Research Center
Moffett Field, California 94035

N80-23250**

LEEWARD FLOW OVER DELTA WINGS AT SUPERSONIC SPEEDS

Joachim G. Szodruch,* and David J. Peake**

Ames Research Center

ABSTRACT

A survey is made of the parameters affecting the development of the leeward symmetric separated flow over slender delta wings immersed in a supersonic stream. These parameters include Mach number, Reynolds number, angle of attack, leading-edge sweep angle, and body cross-sectional shape, such that subsonic and supersonic leading-edge flows are encountered. It is seen that the boundaries between the various flow regimes existing about the leeward surface may conveniently be represented on a diagram with the components of angle of attack and Mach number normal to the leading edge as governing parameters.

Although the work in this field has been mainly experimental over the last twenty-five years, recent laminar-flow computations using approximate forms of the Navier-Stokes equations have provided details of the flow field that are in reasonable agreement with experimental results at low Reynolds numbers.

LIST OF SYMBOLS

C_D drag coefficient

C_L lift coefficient

C_p pressure coefficient = $\frac{(p - p_\infty)}{0.7 p_\infty M_\infty^2}$

L maximum wing chord

M Mach number

R_{L_∞} Reynolds number based on chord length and free-stream conditions

r leading-edge radius

s local semispan

t maximum thickness of wing

*Research Associate.

**Consultant, 3-D Flowz, Inc., P.O. Box 244, Moffett Field, Calif. 94035.

U velocity in X direction
 X^* distance downstream from wing apex
 $\left. \begin{matrix} X \\ Y \\ Z \end{matrix} \right\}$ coordinates with origin at wing apex, see Fig. 3
 α angle of attack, measured between wind vector and leeward generator in meridian plane
 β angle between leeward meridian (ridge line) and X axis
 θ_{A1} primary attachment line
 θ_{A2} secondary attachment line
 θ_{S1} primary separation line
 θ_{S2} secondary separation line
 θ_{S3} tertiary separation line
 Λ leading-edge sweep angle
 λ angle between leading edge and X -axis ($= 90^\circ - \Lambda$)
 χ hypersonic viscous interaction parameter $= M_\infty^3 / \sqrt{R_{L_\infty}}$
 ψ angle between upper and lower surface, in plane normal to leading edge

Subscripts:

∞ free-stream conditions
 N conditions normal to leading edge

1. INTRODUCTION

The flow field over a slender delta wing at angle of attack immersed in a supersonic stream can be divided into two characteristic regions. The windward or pressure side faces the oncoming flow and is strongly influenced by the bow shock wave; the leeward or suction side is dominated by the effects of viscous/inviscid interaction. It is the leeward flow that forms the subject

of the following survey. Especially in the last decade, interest has increased in measuring and predicting the flow about low aspect ratio wings, with the operation of the supersonic transport aircraft "Concorde," as well as the development of the hypersonic Space Shuttle. In spite of there being a large amount of literature on the subject (see also Smith 1975 and Stahl 1979), only recently have efforts been made to catalog the details of the lee-side flow regimes (Stanbrook and Squire 1964; Squire 1976; Szodruch 1977; Peake and Tobak 1980).

Apart from the simple solution where at low angles of attack the leeward flow over the entire wing is virtually attached, two types of essentially conical¹ symmetric separated flow have been recognized at larger angles of attack, depending on whether the leading edge is outside or inside the Mach cone from the apex. The first is the well-known case of "leading-edge separation," which is also found at subsonic speeds for wings with sharp, swept leading edges. Here, the flow, in turning from the lower, high-pressure side to the upper surface, separates at the leading edge forming counter-rotating spiral vortices. The second type of flow is known as "shock-induced separation," where the flow is supersonically expanded around the leading edge and is deflected towards the centerline of the wing. Now, due to symmetry requirements, the flow is turned parallel to the free-stream direction by means of inboard embedded shock waves. If the shock waves are strong enough, their adverse spanwise pressure gradients cause the three-dimensional boundary layer to separate and again form counter-rotating spiral vortices. But note, whereas the separation lines are situated at the leading edge in the subsonic cross-flow case, they are inboard of the leading edge in the supersonic example. These flow fields and their associated skin-friction line patterns are sketched in figure 1(a) and appear over simple delta wings as well as over more complicated shapes like the "Concorde" (Collard 1978) or the Space Shuttle (Bornemann and Surber 1978). Since vortices (with or without embedded shock waves) occur over the wing at virtually every flight condition and are also a useful source of lift, the essential issue of design with slender wings is to fix the location of the separation lines so that the vehicle is always controllable (Peake 1976).

At hypersonic speeds, the flow types appear somewhat similar, although the flow in most cases is no longer conical in the "strong" hypersonic viscous interaction regime. Hypersonic viscous interaction (characterized by the parameter $\chi = M_\infty^3 / \sqrt{R_{L_\infty}}$) then becomes important, especially near the wing apex, and the vortices induce high rates of heat transfer along attachment lines. Some typical types of flow for this hypervelocity regime are sketched in figure 1(b). While three of the flow fields shown in figure 1(b) appear analogous to those in figure 1(a), the one called "attached leading-edge flow with vortices" is considered to be an additional flow pattern at hypersonic speeds for wings at low angles of attack with transitional boundary layers. Here, a vortex system is considered to form within the "two-layer"² boundary layer near

¹Either fully laminar or fully turbulent.

²With viscous layer very close to the wall and essentially inviscid outer layer.

the wing apex. Due to the form of the lateral pressure gradients, the inner low momentum flow and the outer layer with near inviscid conditions respond at different rates of skew, thereby developing a shear layer between them which finally rolls up into "embedded vortices" (Rao and Whitehead 1972). A detailed survey of flows about slender delta wings at hypersonic Mach numbers is given by Dunavant et al. 1976.

The purpose of the present survey is to find a common basis for the different experimental and essentially conical flow results so far obtained for delta wings at supersonic speeds. The influence of parameters such as Mach number, Reynolds number, angle of attack, leading-edge sweep angle, and body cross-sectional shape on the form of the leeward flow field will now be discussed in detail.

The authors wish to thank Murray Tobak for his review of the text and the constructive discussions with him throughout the course of the study.

2. FLOW TYPES AND BOUNDARIES

A list of experiments selected for review is shown on the chart in figure 2. Here, one sees that the major part of the research effort has concentrated on thin³ delta wings with flat upper surfaces and high leading-edge sweep angles. For the purpose of systematizing the flow, we shall assume that the flow conditions are essentially conical.⁴ It then appears sufficient to describe the flow in a plane normal to the leading edge, using the parameters of Mach number and angle of attack decomposed into components in that plane. These components, M_N and α_N , are:

$$M_N = M_\infty \sqrt{1 - \sin^2 \Lambda \cdot \cos^2(\alpha + \beta)}$$

$$\alpha_N = \tan^{-1} \frac{\tan(\alpha + \beta)}{\cos \Lambda} - \tan^{-1} \frac{\tan \beta}{\cos \Lambda}$$

where Λ is the leading-edge sweep angle and β is the upper surface wedge angle in the plane of symmetry. The angle of attack α is measured in the meridian plane between the wind vector and the ridge line (the leeward generator) on the upper surface. The parameters M_N and α_N , which are taken to characterize the flow field, are illustrated in figure 3. For a flat-topped delta wing with $\beta = 0^\circ$, the equations reduce to those given by Stanbrook and Squire (1964). It should be noted that this concentration on the normal components, α_N and M_N , while making sense for sharp-edged wings, cannot be used for the closely allied case of cones. Thus, a criticism against the rationale is that cones and delta wings cannot be brought into the same system of classification, even though the flow topology is analogous (Tobak and Peake

³Thickness-to-chord ratio typically less than 0.1.

⁴Conditions on the surface and in the flow field along a ray from the wing apex are constant.

1979). We remember that in incompressible flow, the parameters of relative incidence⁵ α/θ_c , α/λ , and cross-flow velocity $U_\infty \sin \alpha$, have been used to correlate, respectively, cone or delta wing results.

2.1 The α_N vs M_N Diagram

In flight, there are two principal parameters of interest which strongly influence the flow field above the wing: the Mach number M_∞ and the angle of attack α . For the delta wing under discussion, we consider only the components normal to the leading edge, i.e., M_N and α_N . In 1964, Stanbrook and Squire evaluated the available experimental results in an α_N vs M_N diagram, defining regions of attached and separated flow at the leading edge. The boundary between these two regions has since been called the "Stanbrook-Squire Boundary." We shall abbreviate this term to SSB in the ensuing text. Notice that although we are assuming that the sweep angle Λ can be effectively removed as a governing parameter by utilizing the formulation for α_N and M_N , no explicit experiments have been conducted with models of varying sweep angle and in streams of varying M_∞ to verify that identical flow fields are produced at particular coordinates α_N , M_N . Figure 4 shows experimental results for rounded (fig. 4(a)) and sharp (fig. 4(b)) leading edges, together with other results for wing-body combinations (Squire et al. 1961) and the Space Shuttle (NASA 1972). It is clear from figure 4 that the shape of the leading edge plays an important role in the development of the flow field over the wing. As a consequence, when the attempt is made to systematize the flow types for wings with different leading-edge radii, a broad region results where both separated and attached flows may be found in the α_N vs M_N diagram. In the present report, emphasis is placed on wings with sharp leading edges. The zone between separated and attached leading-edge flow representing the limits for the changeover from one flow type to the other, is then a narrower band in figure 4(b) than the comparable band in figure 4(a). The experimental investigations carried out thus far have employed well-established techniques such as static and pitot-pressure measurements, heat-transfer measurements, and, very importantly, flow-visualization techniques in the flow and on the surface. However, since most experiments are conducted with relatively small models, a careful interpretation of the results is usually required. Figure 5(a) shows the skin-friction line pattern and form of the external flow for the case of leading-edge separation at moderate angle of attack. The conical lines of separation and attachment are denoted on the leeward surface by angles θ_S and θ_A , respectively. Figure 5(b) shows the details of the flow field when the flow is attached at the leading edge but separates inboard (the "shock-induced" type). The difference between attached and separated flow at the leading edge is evident from the skin-friction line pattern on figure 1. When the flow is attached, the local direction of the skin-friction lines is away from the leading edge; when it is detached, the converse is true. The investigations of Szodruch (1977) show that the flow type may also be detected from the location of the (primary) vortex core above the wing. Results for the positions of the primary vortex core, the primary attachment line, and the

⁵The cone semi-nose angle is θ_c ; the semi-angle at the wing apex is λ .

secondary vortex core are shown in figure 6. Three different Mach numbers are illustrated, representing the regions to the left ($M_\infty = 2$ and 2.5 in figs. 6(a) and 6(b), respectively) and to the right ($M_\infty = 3.5$ in fig. 6(c)) of the SSB. If the normal component of Mach number is substantially less than one, the path of the primary vortex core, as angle of attack is increased, is shown in the upper diagram (fig. 6(a)). This is the typical behavior also in incompressible flow and is compared with results of calculations by Pershing (1964) who used inviscid approximations to model the leeward flow. At higher free-stream Mach numbers, but still to the left of the SSB (fig. 6(b)), the primary vortex core follows a path similar to that shown in figure 6(a); but this result applies only up to angles of attack where the SSB is entered. To the right of the SSB, a further increase in free-stream Mach number results in positions of the primary vortex core occurring very close to the wing (see the lower diagram, fig. 6(c)). Note that in the experimental results for the rather thick wings⁶ shown in figure 6, the primary vortex core position remains virtually invariant at all free-stream Mach numbers for angles of attack up to $\alpha = 5^\circ$. In contrast, at higher angles of attack, the position of the primary vortex core is dependent on free-stream Mach number. Figure 7 presents again the results of figure 6 and supportive results from other investigations of the spanwise primary vortex position plotted against normal angle of attack. There is an apparent relationship between the core location and the type of leading-edge flow, whether attached or separated, in the range of Mach numbers covered, $0 \leq M_\infty \leq 4$. Within the shaded area in figure 7 (which is the SSB), both types of flow occur.

The results discussed so far, and further detailed studies of Szodruch and Ganzer (1978) and Szodruch (1977), lead to the following concise description of the types of flow in the α_N vs M_N diagram, figure 8. As can be seen in figure 8, the respective flow regions are numbered 1 to 6. The original SSB is shown in addition to three new regions identified by Szodruch (1977) (regions 3, 4, and 6) in his experiments with flat-topped thick wings of thickness-to-chord ratio 0.25. These new regions will also be discussed by describing the change of flow type that occurs when the Mach number or angle of attack varies. In addition, reference will be made to trajectories nominally parallel to the SSB (labelled AA, BB) and across the SSB (labelled CC). The influence of other parameters, such as Reynolds number and body cross-sectional geometry, will be considered later in section 2.2.

Looking in more detail to the region on the left (region 2) of the SSB on figure 8, we choose a fixed free-stream Mach number (say $M_\infty = 2$ with $\Lambda = 73^\circ$) and follow a line with increasing angle of attack AA, starting at $\alpha_N = 0^\circ$. Because of the thickness of the wing, the flow separates in turning around the sharp leading edge from the lower to the upper surface at zero and at all positive angles of attack. Thus, leading-edge separation is found over the entire angle of attack range investigated, $0^\circ < \alpha < 30^\circ$. As already shown in figure 6(a), the primary vortex first moves inboard until it reaches a position equal to about half the semispan and then, with further increase in angle of attack, returns towards the leading edge. Also, the distance of the vortex core from the upper surface increases and the overall size of the

⁶Thickness-to-chord ratio = 0.25.

vortex grows until almost the entire semispan is covered. For the present thick wing and sweep angle $\Lambda = 73^\circ$, a secondary vortex may be detected only at angles of attack within the range $10^\circ \leq \alpha \leq 20^\circ$ (see fig. 6(a)).

When the primary vortices become close together at very high angles of attack (see region 1 on fig. 8), there is a new development in the cross-flow structure. Because of the strong downwash induced by the primary vortices at and close to the meridian plane, the crossflow accelerates to a supersonic velocity through the resulting convergent-divergent stream tube. As the crossflow must then tend toward zero as the leeward surface is approached, it consequently decelerates through a local normal shock wave. This so-called centerline shock wave lies virtually parallel and very close to the upper surface. Little is known about the real conditions across the shock wave, because of its close proximity to the model surface and the difficulty in using probe instrumentation which may disturb the flow field. The centerline shock has been observed in a limited number of investigations and appears not only above the delta wing (Monnerie and Werlé 1968; Szodruch and Ganzer 1978) but also above cones (Nebbeling and Bannink 1976). The shock has been observed at Mach numbers between $M_\infty = 2$ and 3, and angles of attack from $\alpha = 20^\circ$ to 30° (Monnerie and Werlé 1968; Nebbeling and Bannink 1976; Szodruch and Ganzer 1978).

Still in figure 8, we now consider a Mach number M_∞ such that with increasing angle of attack the wing encounters the flow fields on the right-hand side of the SSB (say $M_\infty = 4$ with $\Lambda = 73^\circ$). Reference should be made to the trajectory BB. The flow around the leading edge may still be subsonic at low angles of attack. Starting at $\alpha_N = 0^\circ$, "leading-edge separation" is observed for thick wings (Szodruch 1977) which is not in agreement with the thin wing results of Stanbrook and Squire (1964). Upon increasing the normal angle of attack α_N from 16° to 25° ($5^\circ < \alpha < 8^\circ$), the vortex core moves rapidly towards the leeward meridian (see also fig. 6(c)). The flow around the leading edge behind the detached shock wave is now nominally supersonic. Within the precision available from the experimental observations, Szodruch (1977) considered separation to occur very close to the leading edge but just inboard of it concomitant with a sudden, but local flow deceleration. The crossflow then reaccelerates and diffuses subsequently through a weak shock-wave structure located above the vortex. In figure 8 this flow regime 4 is labelled "separation with shock." The terminology of Narayan (1978) for region 4 is "attached leading-edge flow with vortices" (see fig. 1(b)), the weak shock formation distinguishing this flow regime 4 from the strong "shock-induced separation" zone 5. Further increase in angle of attack does not seem to alter the flow type, but the vortex size does expand. Rao and Whitehead (1972) characterized region 4 at low angles of attack as being one with attached flow at the leading edge with vortices "embedded" within the viscous flow but commencing some distance downstream of the apex. The view of Rao and Whitehead (1972) would appear to be consistent with the observation of transitional flow containing streamwise vortices recorded in Maltby (1962) and by McDevitt and Mellenthin (1969). At very high angles of attack, the flow is difficult to characterize from wind-tunnel experiments, because the vortices become particularly sensitive to the high static pressures induced in the wake by reflected shock waves, support-strut interference, and flow probes. Vortex

breakdown may occur, causing significant changes in the leeward flow at free-stream Mach numbers typically up to $M_\infty = 3.5$ (Szodruch 1976; Richards 1976).

Finally, in figure 8, let us fix the normal angle of attack α_N at 21° ($\alpha = 7^\circ$ with $\Lambda = 73^\circ$) and gradually increase the normal Mach number component M_N . We now follow the horizontal trajectory CC in the α_N vs M_N diagram. At low values of M_N , "leading-edge separation" with primary and secondary vortices is observed with a primary attachment line outboard of the leeward meridian (Θ_A in fig. 5). As M_N increases, the vortices tend to flatten and move towards the meridian with no significant change in position of the primary attachment line. The strength of the primary vortices decreases, as is inferred from a reduction in peak suction pressures. Within the SSB it is not possible to detect the formation of secondary vortices. Crossing region 4 and with increasing M_N , we finally enter region 5 in which flow separation is of the "shock-induced" type. In regions 4 and 5, we remember that the flow is attached at the leading edge. The "shock-induced separation" typical of these regimes exists, however, only for moderate angles of attack. If, in figure 8, we now allow the normal angle of attack to increase substantially at the end point of trajectory CC, the flow becomes that in region 6 with, once again, separation at the leading edge. The resulting boundary is discussed by Squire (1976), who argued that the flow change about the leeward surface is related to the flow conditions on the lower surface. Accordingly, it is the leading-edge angle ψ (i.e., the angle between the upper and lower surfaces normal to the leading edge) which determines the values of α_N at which the change occurs from "shock-induced separation" in region 5 to "leading-edge separation with shock" in region 6.

2.2 Influence of Reynolds Number and Body Cross-Sectional Geometry

The parameters that influence the structure of the leeward flow over a delta wing are divided into two groups. In the first group, we have the stream conditions Mach number and Reynolds number. The second group accounts for the attitude of the wing relative to the flow, and includes the angle of attack, the sweep angle, the leading-edge angle, the cross-sectional shape, and the degree of leading-edge rounding. In the previous section, we have already introduced the leading parameters of each of the two groups, Mach number and angle of attack, that cause the most severe changes in the flow field. Now we consider the influence of the remaining parameters of the two groups: first, Reynolds number, and then the collection of parameters that describe the body geometry.

The influence of Reynolds number on the flow has been given more attention at hypersonic speeds than at supersonic speeds. This is because the effects of Reynolds number on peak heating as well as on the development and size of characteristic patterns in the flow field are more important at high velocities (Dunavant et al. 1976; Rao and Whitehead 1972). It is apparent that under leading-edge flow conditions from hypersonic to subsonic, when flow separation is fixed at the leading edge (regions 6, 3, 2, and 1 in fig. 8), Reynolds number has little effect on the primary vortex structure. In contrast, since the secondary separation lines are not fixed, the disposition of the secondary vortices may be influenced by Reynolds number to a larger extent

(for example see Hummel and Redeker 1972). For purposes of illustration, the locations of the secondary separation lines vs Reynolds number are plotted for supersonic as well as subsonic free-stream Mach numbers on figures 9(a) and (b), respectively. There is a noticeable movement of the secondary separation line position towards the leading edge as Reynolds number $R_{L\infty}$ increases from 10^4 to 10^7 . These results imply that boundary-layer transition and the associated longitudinal vortices developing from amplifying instabilities in the laminar zone (Maltby 1962; Ginoux 1967) may be exerting an important influence on the development of the leeward flow. As angle of attack increases to higher values, the transition zone moves closer to the wing apex, so that any effect of transition becomes less at the measurement station shown on figures 9(a) and (b). The consequence is a slowdown in the rate of movement of the secondary separation line position in the turbulent flow. We should note that the form of the static pressure distribution across the wing semispan attributed to the primary vortex evidences an increase of the peak suction pressure level as we proceed from laminar to turbulent flow. Correspondingly, the effect of the secondary vortices on broadening the width of the suction pressure zones is greater in laminar than in turbulent flow (Hummel 1965; Küchemann 1975; NASA High Reynolds Number Research 1977).

In figure 8 we have introduced the various flow regions existing on the right-hand side of the SSB. Figures 10 and 11 illustrate the effect of Reynolds number at, respectively, a nominally constant α_N and at a nominally constant M_N , on the disposition of the boundaries between these given flow regions for both thin and thick wings. With α_N fixed at about 28° , figure 10 shows that as Reynolds number increases, the effects of transition (with longitudinal vortices, Rao and Whitehead 1972) in region 4 diminish until at sufficiently high Reynolds number ($R_{L\infty} = 10^7$), region 4 can no longer be ascertained. The flow field develops directly from one with leading-edge separation for $M_N < 1$ (region 2) to one with shock-induced separation for $M_N > 1$ (region 5). In figure 11, with Mach number fixed at a sufficiently high value ($M_N \sim 2.5$) and fixed α_N also sufficiently large, the effect of increasing Reynolds number is to alter the flow field from one with strong shock-induced separation (region 5) to one with leading-edge separation (region 6). Increase of Reynolds number evidently causes a thinning of the boundary layer developing from the leading edge, thereby generating a larger turning angle in the Prandtl-Meyer expansion fan around the leading edge. The consequence is a stronger shock wave above the wing and a movement of the primary separation line towards the leading edge (Narayan 1978). Thus, the few available data indicate that Reynolds number has a strong effect on the location of the boundary between regions 4 and 5 and between regions 5 and 6 in the α_N vs M_N diagram. Figure 8 is therefore strictly valid only for one Reynolds number, as Szodruch (1978) had demonstrated earlier.

Let us now consider the effect of changing body cross-sectional geometry. The leading edge angle ψ lies in a plane normal to the leading edge between the upper and lower surfaces (see fig. 3) and thus, for the triangular cross section, determines the thickness of the wing. The degree of influence of ψ on the flow depends on which region in the α_N vs M_N diagram we pinpoint. On the left-hand side of the SSB in figure 8, a change of ψ from, say, 5° to 40° seems to have no effect on the type of leading-edge flow separation. On the other hand, for the same range of ψ (at $\Lambda = 75^\circ$ and $M_\infty \sim 2$),

figure 12(a) indicates that ψ has a considerable influence on the leeward boundary-layer development, as inferred from the positions of the secondary separation lines. The typical trajectory along which we wish to sweep is once again AA in figure 8. Once the angle of attack α exceeds about 15° ($\alpha_N \sim 40^\circ$), we see that the positions of the lines of secondary separation move more rapidly towards the leading edge on the thick wings ($26^\circ < \psi < 90^\circ$) than they do on the thin-wing examples ($5^\circ < \psi < 15^\circ$). The influence of increasing Reynolds number, shown previously in figures 9(a) and (b), was also seen to drive the lines of secondary separation towards the wing leading edge. On figure 12(a), however, we note that the test conditions for the thick wings were at lower Reynolds numbers than for the thin wings, so that the results on figure 12(a) are considered representative of changing the geometry of the wing lower surface.

On the right-hand side of the SSB on the α_N vs M_N diagram of figure 8, the parameter ψ has a major influence on the flow development, especially in region 3. It has to be noted, however, that at low angles of attack in this region, some carefully conducted experiments by Ginoux (1967) have shown that other conditions at the leading edge, such as bluntness and roughness, contribute to the formation of longitudinal vortices, thereby modulating the structure of the viscous flow on the upper surface. Figure 12(b) illustrates the secondary separation line positions for the regions traversed by a typical trajectory such as BB in figure 8. The free-stream Mach number is $M_\infty \sim 3.5$, and the range of angle of attack is $0^\circ < \alpha < 30^\circ$. At high angles of attack, figure 12(b) illustrates that the discernible trend in movement of the line of secondary separation towards the leading edge for the thick wings corresponds with that in figure 12(a); in addition there is also a substantial movement of the line of secondary separation in the same direction at low angles of attack. Only for the flow in region 4 (the center of the graph) do the results for positions of the line of secondary separation for both thin and thick wings appear in close proximity. Here the flow is supersonic around the leading edge, and the respective flow regions about the lower and upper surfaces can, for all practical purposes, be considered independent (Squire 1976). If the cross-sectional shape of the flat-topped delta wings is other than triangular, for instance, with re-entrant corners in the underside surfaces, then viscosity will play a large part in the flow development not only on the leeward surface, as presently discussed, but on the windward surface in addition (Peake and Tobak 1980).

The boundary in the α_N vs M_N diagram at high angles of attack (between regions 5 and 6 in fig. 8), where the flow changes from the shock-induced separation type to the leading-edge separation type is strongly dependent on ψ . This dependence is clearly brought out by the calculated results of Squire (1976) shown in figure 13. It is seen that the boundary between regions 5 and 6 falls in terms of normal angle of attack in proportion as the leading edge angle ψ rises. Also plotted in figure 13 are results from experimental studies that appear to support the calculations, notwithstanding the variation in Reynolds number between the experimental results at a given ψ (compare with fig. 11).

In general, it has to be noted that in most experimental and theoretical investigations, there is a lack of data near the leading edge or close to the

apex. The reason lies in the insufficient power of resolution of instrumentation as well as of computation. This is unfortunate, since it seems to be of great importance to have a physical understanding of the flow development in these regions (Tobak and Peake 1979). In our own experiments (unpublished results of Szodruch), nonconical regions were observed near the apex even under conditions for leading-edge separation, although the overall flow field appeared to be conical. The cause is attributed not only to viscous interaction, but to imperfections in manufacturing the models such as rounding the sharp edges and the apex, and also to effects of Reynolds number and leading-edge angle. In figure 14, the length of attached flow at the apex, X_1^* , is plotted vs angle of attack for the flow region 2 on the left-hand side of the SSB (fig. 8). The models are those tested by Szodruch (1978). Graphs for values of ψ of 20° and 40° are illustrated at two Reynolds numbers. We note that X_1^* diminishes with increasing angle of attack, Reynolds number, and leading-edge angle, allowing the flow field to approach conical conditions of leading-edge separated flow. (The separation lines start in the nose region from saddle singular points in the pattern of skin-friction lines which, due to grain size in the oil flow, could not be discerned. It should be noted that sequences of flow structures in the nose region as angle of attack is increased are postulated by Tobak and Peake (1979).)

Finally, the extent of rounding of the leading edge is also a parameter in the choice of body cross-sectional geometry. An increase in leading-edge radius from sharp to, say, 1% of maximum chord length, does not significantly affect the lift/drag performance at supersonic speeds, but does improve it at subsonic and transonic Mach numbers (Morris et al. 1978; Bashkin 1967; Bobbitt and Manro 1976).

3. NONFLAT LEEWARD SURFACES

So far, delta wings with flat leeward surfaces have been considered. In the following, a brief description of the leeward flow over nonflat wings is given, where, according to figure 3, the wedge angle is $\beta > 0^\circ$. Only straight leading-edge planforms will be discussed. Flows over cones and other shapes such as the Space Shuttle have been reported, for example, in Peake and Tobak (1980) and in the NASA Space Shuttle Aerothermodynamics Technology Conference 1972. Let us note that the angle of attack is now measured with respect to the ridge line and no longer with respect to the plane containing the leading edges. This is done so that at positive angles of attack the upper surface is in the lee of the free-stream flow. The flow regions denoted as "leading-edge separation" and "shock-induced separation" (regions 2 and 5 in fig. 8), are also found about nonflat wings. Figure 15 shows spanwise static pressure distributions on a delta wing whose ridge line deflection is $\beta = 8^\circ$ (Küchemann 1964) for a sequence of increasing values of M_∞ (or M_N). The angle of attack is 2° (equivalent to a value of $\alpha_N = 5.3^\circ$). In the α_N vs M_N diagram (fig. 8), therefore, we move along a trajectory parallel and close to the abscissa.

Leading-edge separation occurs for Mach numbers M_∞ between 1.3 and 2.8 ($M_N < 1$) with noticeable suction peaks induced by the primary vortices. The

flow field changes to one with marginally shock-induced separation, as implied by the monotonic increase in static pressure inboard of the leading edges, once M_∞ reaches 4 ($M_N = 1.18$). Note the contrast with the results for the flat-topped wing at low angle of attack, illustrated in figure 8, wherein leading-edge separation existed across the SSB, from region 2 to region 3. Hence, deflecting the ridge line of the wing top surface potentially alters the boundaries of the regions exhibited in the α_N vs M_N diagram. Some additional results from another model with the ridge line deflection increased to 14.5° and with a flat underside are displayed in figure 16. Here, contours of constant pitot pressure ratio are drawn in crossflow planes on the leeward side of the wing. The presentation of results follows a trajectory on the α_N vs M_N diagram (see fig. 8) corresponding roughly with AA, but curving into the SSB at $\alpha_N > 15^\circ$. The noticeable feature is that even though $M_N > 1$ at moderate values of α_N , leading-edge separation is witnessed in the pitot contour patterns at $M_N = 1.13$ and 1.20 . Secondary separation lines are also well defined on the wing top surface. Once $M_N > 1.4$, however, the primary separation line moves inboard consistent with shock-induced separation at all remaining but increasing Mach numbers. The pitot contours in proximity to the enshrouding shock wave about the wing are also identifiable in figure 16.

Other results for the inverted triangular cross-section wing, such as oil-flow visualization and Schlieren, along with those already discussed, allow us to draw a new α_N vs M_N diagram in figure 17 for a wing with a deflected ridge line of $\beta = 14.5^\circ$. We detect that in comparison with figure 8 for flat-topped wings, and measuring angle of attack with respect to the ridge line, the SSB shifts to the right by about $\Delta M = 0.4$. The α_N vs M_N diagram in figure 17 essentially duplicates the one drawn by Stanbrook and Squire (1964) for basically flat-topped wings. For this wing with deflected ridge line, only regions of leading-edge separation and shock-induced separation are found. At free-stream Mach numbers greater than 3.5, the leeward flow becomes nonconical, possibly as a result of base-flow interference (observed as a deviation of the separation lines from conical rays on the rear part of the wing), but certainly because of viscous interaction when deviations are detected in the region of the wing apex as we see in figure 18. Here, as in figure 14, we plot X_1^* as the chordwise position where the skin-friction lines essentially return to a conical display. The results in figure 18 are for high free-stream Mach numbers of 6 and 9. In view of the viscous interaction parameter χ , which is proportional to M_∞^3 , we must expect a larger nonconical region at higher Mach numbers, as figure 18 vividly shows. It should be noted that at these hypersonic Mach numbers, various experimenters (e.g., Rao and Whitehead 1972) have found similar trends for flat-topped wings.

4. SOME COMPARISONS WITH COMPUTATIONAL RESULTS IN LAMINAR FLOW

Some comparisons will be made between experimental results and results of recently developed laminar-flow computational methods. The flow over the lower surface is not discussed further, since extensive information about this part of the problem is available (e.g., Fowell 1956; Babayev 1963; Squire 1968; and Kutler and Lomax 1971). However, computational methods involving detached bow shock waves must take account of the flow on the pressure side because the

two sides are not independent. In general, the computational methods can be divided into two groups according to their application on delta wings with either subsonic or supersonic leading edges. In these two respective groups, the flow cases of leading-edge separation and shock-induced separation are treated.

There are a number of methods available for computing flows involving leading-edge separation; a comprehensive review is given by Parker (1976). However, no computational model adequately predicts all aspects of the flow development. Techniques such as the leading-edge suction analogy, potential flow theory with slender body assumptions, or where the flow is modeled by two concentrated vortices, may yield results which predict one feature of the flow reasonably well (e.g., overall forces, spanwise loading, vortex position, etc.), but fail to predict the others. Two recent investigations introduce methods which take account of another flow aspect, the occurrence of local supersonic regimes for wings with subsonic leading edges. These methods give solutions of the nonlinear, steady, inviscid potential equations (Grossman 1978; Grossman and Siclari 1980) and of the rotational, nonlinear, inviscid Euler equations (Siclari 1979). Results from both agree quite well with each other except for minor differences in static pressure level and embedded shock-wave location. Notwithstanding, good agreement with experiments is demonstrated only at small angles of attack, where there is no or only a small local supersonic region developed in the calculation. The disagreement otherwise is to be expected in view of the attempt to solve the viscous problem with inviscid flow equations. According to the α_N vs M_N diagram, the flow discussed in Grossman (1978) and Siclari (1979) is expected to show separation at the leading edge for all positive angles of attack. The Navier-Stokes equations take care of these kinds of flow fields, and in Vigneron et al. (1978), two numerical approaches utilizing approximate forms of the equations are undertaken to obtain solutions for a flat-topped delta wing. Figure 19 shows a typical example from these computations where the velocity vectors have been plotted in the wing crossflow plane; the vortex center, separation, and attachment lines are indicated. Comparison between calculated and experimental pressure distributions across the semispan are presented in figure 20. The calculated pressures on the lower surface show very good agreement with experimental results when the correct leading-edge angle ψ is used. On the upper surface, results from the inviscid methods of Grossman (1978), and similarly those of Siclari (1979), show a sharp pressure rise at the location of the embedded shock wave. The experiment, however, reveals leading-edge separation with primary and secondary vortices and with no embedded shocks, as shown in figure 20. The solution of Vigneron et al. (1978), on the other hand, shows good correspondence with the actual physics (see fig. 19) of the flow including the location of the primary and secondary vortices, but the vortex-induced peak pressure and the pressure beneath the attached flow adjacent to the meridian are, respectively, under- and over-predicted. However, it has to be noted that the wing geometries in the three investigations are not exactly identical (in leading-edge angle, sweep angle, leading-edge radius); therefore, minor differences are to be expected.

In figure 21, the influence of angle of attack on the flow field is presented for calculated and experimental results at a free-stream Mach number of 2.0. In figure 21(a), the shock position obtained from the inviscid flow

calculations moves inboard with increasing angle of attack and, in general, is not in agreement with the experimental results. Since at higher angles of attack the vortex again moves towards the leading edge while the shock moves in the opposite direction to positions further inboard, no agreement at all is to be expected between the inviscid flow theory and the experimental results. The vortex or shock strength can be related to the pressure difference between the meridian plane value and the peak suction level; the resulting pressures are plotted in figure 21(b). The inviscid flow results overpredict the pressure difference except at small angles of attack where the local supersonic region has not yet developed near and at the leading edge. But neither does the viscous method yield results that agree with the experimental measurements, although these calculated (viscous) results are closer to experiment. Despite these differences, the computed (viscous) results of Vigneron et al. (1978) are promising, and further test cases and parameter variations are highly desirable. We note that a rough estimation of the pressure development is represented by the solid line in figure 21(b), where the pressure difference is calculated assuming a Prandtl-Meyer expansion in the meridian plane coupled with an expansion around the leading edge in the crossflow plane.

The influence of free-stream Mach number on the calculated results is again tested by evaluating the position of the primary vortex core above the wing and the pressure rise across the semispan for a flat-topped delta wing with $\Lambda \sim 73^\circ$ at $\alpha \sim 10^\circ$. Comparisons between computed and experimental data are shown in figures 22(a) and (b). Rather good agreement is achieved over the entire Mach number range, especially with the inviscid methods. This is expected, since at higher velocities, shock-induced separation occurs, and the inviscid flow methods (Grossmann 1978; Siclari 1979) are closer to the actual flow physics than for the lower Mach number case previously discussed. Results from another inviscid flow method due to Szodruch (1977) are also presented. In this method, the inviscid flow field is solved taking into account the viscous part and the detached bow shock wave by means of semi-empirical equations.

The flow over thin planar delta wings with supersonic leading edges and laminar boundary-layer flow has been computed by Bluford (1978) employing approximate forms of the unsteady Navier-Stokes equations. At supersonic free-stream Mach number, this computational method has only been compared with one experiment (Bannink and Nebbeling 1971). This one test case is presented in figure 23. The essential inviscid part of the flow field agrees rather well with the experiment (see also Voskresensky 1978, and Walkden et al. 1974). However, according to the α_N vs M_N diagram in figure 8 for this wing configuration, shock-induced separation is expected, while the computation yields only a weak embedded shock not sufficiently strong to separate the boundary layer. Thus, with further development, the viscous flow computations of Vigneron et al. (1978) and Bluford (1978) offer promise to provide the intricate details of the subsonic and supersonic regions in the leeward flow.

5. CONCLUSIONS

A survey has been conducted of the supersonic flow about slender delta wings. The essential results of the survey are the following:

1. In conical flow we may collapse the flow-field parameters such as free-stream Mach number, wing leading-edge sweep angle, and angle of attack, on to a diagram where the governing parameters are the components of Mach number and angle of attack in a plane normal to the leading edge. Boundaries materialize on this α_N vs M_N diagram to define particular zones of "leading-edge separation" type flows and "shock-induced separation" type flows.

2. The effects of Reynolds number, leading-edge angle, and raising the ridge line at the leeward meridian, modify the locations of the boundaries between the respective flow regimes.

3. Recent computations with approximate forms of the Navier-Stokes equations in laminar flow yield details of the flow structure that are in good qualitative agreement with experimental results. Some further development of the methods and the incorporation of an appropriate turbulence model would appear to be necessary to provide a computational tool for design purposes.

BIBLIOGRAPHY

- Babayev, D. A.: Numerical Solution of the Problem of the Supersonic Flow Past the Lower Surface of a Delta Wing. Translated from Russian in AIAA Journal, vol. 1, Sept. 1963, pp. 2224-2231.
- Bannink, W. J.; and Nebbeling, C.: An Experimental Investigation of the Expansion Flow Field Over a Delta Wing at Supersonic Speed. Rep. VTH-167, Delft Univ. of Techn., The Netherlands, Sept. 1971.
- Bashkin, V. A.: Experimental Investigation of Flow Past Plane Delta Wings at $M = 5$ and Angles of Attack Ranging from 0° to 70° . Akad. Nautik. SSSR, Izvestiya, Mekhanika Zhidkosti i Gaza, no. 3, 1967, pp. 102-108.
- Beeman, E. R.; and Powers, S. A.: A Method for Determining the Complete Flow Field Around Conical Wings at Supersonic/Hypersonic Speed. AIAA Paper 69-646, 1969.
- Bluford, G.: A Numerical Solution of Supersonic and Hypersonic Viscous Flow Fields Around Thin Planar Delta Wings. AFFDL TR-78-98, Sept. 1978.
- Bobbitt, P. J.; and Manro, M. E.: Theoretical and Experimental Pressure Distributions for a 71.2° Swept Arrow Wing Configuration at Subsonic, Transonic, and Supersonic Speeds. NASA CP-001, part 1, paper 5, Nov. 1976.
- Bornemann, W. E.; and Surber, T. E.: Aerodynamic Design of the Space Shuttle Orbiter. AGARD CPP-247, paper 11, Sept. 1978.
- Brown, C. E.; and Michael, W. H.: On Slender Delta Wings with Leading Edge Separation. NACA TN 3430, April 1955.
- Collard, D.: Comportement à haute incidence d'un avion de transport à aile à grand élanement (Behavior of an aircraft with slender wings at high angles of attack). AGARD CPP-247, paper 10, Sept. 1978.
- Collis, D. C.: A Hypersonic Wind Tunnel Study of a Thick Delta Wing. Note ARL/A. 232, Australian Defence Sci. Service, Melbourne, Nov. 1964.
- Craven, A. H.; and Alexander, A. J.: An Investigation of Vortex Breakdown at $Mach = 2$. Cranfield Co A, Note Aero 158, England, Nov. 1963.
- Cross, E. J.: Experimental and Analytical Investigation of the Expansion Flow Field Over a Delta Wing at Hypersonic Speeds. ARL 68-0027, Aerospace Research Lab., Feb. 1968.
- Drougge, G.; and Larson, P. O.: Pressure Measurements and Flow Investigations on Delta Wings at Supersonic Speeds. The Aeronaut. Res. Inst. of Sweden, FFA Rep. 57, 1956.


- Dunavant, J. C.; Narayan, K. Y.; and Walberg, G. D.: A Survey of Lee Side Flow and Heat Transfer on Delta Wing Planform Configurations. AIAA Paper 76-118, Jan. 1976.
- Edwards, J. B. W.: Heat Transfer and Pressure Measurements on the Upper Surface of a Delta Wing at Incidence at Mach Numbers Between 2.0 and 3.6. RAE TR-65144, July 1965.
- Fellows, K. A.; and Carter, E. C.: Results and Analysis of Pressure Measurements on Two Isolated Slender Wings and Slender Wing Body Combinations at Supersonic Speeds. ARA Rep., vol. 1, no. 12, Nov. 1969.
- Fowell, L. R.: Exact and Approximate Solutions for the Supersonic Delta Wing. J. Aeronaut. Sci., vol. 23, no. 8, Aug. 1956.
- Ginoux, J. J.: Instabilité de la Couche Limite sur Ailes en Flèche (Instability of the Boundary Layer on Swept Wings). Zeitschr. für Flugwissenschaften, 15 Jahrgang, Heft 8/9, 1967, pp. 302-305.
- Greenwood, G. H.: Free Flight Measurements of Pressure and Heat Transfer on the Lee Surface of a Delta Wing at Incidence. RAE TR 68 246, Oct. 1968.
- Grossman, B.: A Numerical Procedure for the Computation of Supersonic Conical Flow. AIAA Paper 78-1213, July 1978.
- Grossman, B.; and Siclari, M. J.: The Non-linear Supersonic Potential Flow Over Delta Wings. AIAA Paper No. 80-0269, Jan. 1980.
- High Reynolds Number Research. Workshop at Langley Research Center. NASA CP 2009, 1977.
- Hummel, D.: Experimentelle Untersuchung der Strömung auf der Saugseite eines schlanken Deltaflügels (Experimental Investigation of the Flow Over the Suction Side of a Slender Delta Wing). Zeitschr. für Flugwissenschaften 13, Heft 7, 1965, pp. 247-252.
- Hummel, D.; and Redeker, G.: Experimentelle Bestimmung der gebundenen Wirbelnlinien sowie des Strömungsverlaufs in der Umgebung der Hinterkante eines schlanken Deltaflügels (Experimental Determination of the Bound Vortex Lines as well as of the Flow in the Vicinity of the Trailing Edge of a Slender Delta Wing). Abhandlungen der Braunschweigischen Wissenschaftlichen Gesellschaft 22, 273, 1972.
- Küchemann, D.: On Some Three Dimensional Flow Phenomena of the Transonic Type. In Symposium Transonicum, ed. Oswatitsch, Springer Verlag, 1964, pp. 218-248.
- Küchemann, D.: The Aerodynamic Design of Aircraft — An Introduction, Part 5. RAE Techn. Memo Aero. 1622, Feb. 1975.
- Kutler, P.; and Lomax, H.: Shock Capturing, Finite-Difference Approach to Supersonic Flow. J. Spacecraft, vol. 8, no. 12, Dec. 1972, pp. 1175-1182.

- Lee, G. H.: Note on the Flow Around Delta Wings With Sharp Leading Edges. ARC R&M 3070, 1955.
- Maltby, R. L.: Flow Visualization in Wind Tunnels Using Indicators. AGARDograph 70, April 1962.
- McDevitt, J. B.; and Mellenthin, J. A.: Upwash Pattern on Ablating and Non-ablating Cones at Hypersonic Speeds. NASA TN D-5346, July 1969.
- Michael, W. H.: Flow Studies on Flat Plate Delta Wings at Supersonic Speed. NACA TN 3472, July 1955.
- Minailos, A. W.: Regimes of Supersonic Flow Past Thin Wings. TsAGI, Uchenya Zapiski, vol. 8, no. 4, 1977.
- Monnerie, B.; and Werlé, H.: Étude de l'écoulement supersonique et hypersonique autour d'une aile élancée en incidence (Study of the Supersonic and Hypersonic Flow over a Slender Wing at Angle of Attack). AGARD CP-30, 1968.
- Morris, D. A.; Fuller, D. E.; and Watson, C. B.: Aerodynamic Characteristics of a Fixed Arrow Wing Supersonic Cruise Aircraft at Mach Numbers of 2.3, 2.7, and 2.95. NASA TM 78,706, Aug. 1978.
- Morris, D. W.; and Couch, L. M.: Experimental Pressure Distributions on a Blunt Lifting-Entry Body at Mach 3.71. NASA TN D-4494, April 1968.
- Murray, W. M.; and Stallings, R. L.: Heat Transfer and Pressure Distributions on 60° and 70° Swept Delta Wings Having Turbulent Boundary Layers. NASA TN D-3644, Oct. 1966.
- Narayan, K. Y.: Leaside Flow Field and Heat Transfer of a Delta Wing at $M = 10$. AIAA Journal, vol. 16, no. 2, Feb. 1978, pp. 160-165.
- Nebbeling, C.; and Bannink, W. J.: Experimental Investigation of the Supersonic Flow Field About a Slender Cone at High Incidence. Rep. LR-233, Delft Univ. of Techn., Netherlands, 1976.
- Parker, A. G.: Aerodynamic Characteristics of Slender Wings With Sharp Leading Edges - A Review. J. of Aircraft, vol. 13, no. 3, March 1976, pp. 161-168.
- Peake, D. J.: Controlled and Uncontrolled Flow Separation in Three Dimensions. National Research Council Canada, NAE LR-591, July 1976.
- Peake, D. J.; and Tobak, M.: Three Dimensional Interactions and Vortical Flows With Emphasis on High Speeds. AGARDograph, in press, Feb. 1980. Also NASA TM-81169, Mar. 1980.
- Pershing, B.: Separated Flow Past Slender Delta Wings With Secondary Vortex Simulation. SSD-TDR-64-151, AD 607442, Aug. 1964.

- Rao, D. M.; and Whitehead, A. H.: Lee Side Vortices on Delta Wings at Hypersonic Speeds. AIAA Journal, vol. 10, no. 11, 1972, pp. 1458.
- Reding, J. P.; and Ericsson, L. E.: Review of Delta Wing Space Shuttle Vehicle Dynamics. Paper 30, NASA TM X-2508, 1971.
- Rein, J. A.: Flow Over the Suction Surface of Sharp Edge Delta Wings with Detached Leading Edge Shock Waves. WRE, Techn. Note HSA 102, Australia, Dec. 1964.
- Richards, I. C.: Supersonic Flow Over Low Aspect Ratio Wings. Aero Note 7609, Cranfield Inst. of Techn., England, 1976.
- Siclari, M. J.: Investigation of Cross Flow Shocks on Delta Wings in Supersonic Flow. AIAA Paper 79-0345, Jan. 1979.
- Smith, J. H. B.: A Review of Separation in Steady, Three-Dimensional Flow. AGARD CP 168, paper 31, May 1975.
- Space Shuttle Aerothermodynamics Technology Conference. Ames Research Center, vol. 1, 2, NASA TM X-2506/2507/2509, 1972.
- Space Shuttle Aerothermodynamics Technology Conference. Ames Research Center, vol. 3 - Aerodynamics. NASA TM X-2508, Feb. 1972.
- Squire, L. C.: Pressure Distribution and Flow Patterns on Some Conical Shapes With Sharp Edges and Symmetrical Cross Sections at $M = 4$. ARC R&M 3340, 1963.
- Squire, L. C.: Pressure Distribution and Flow Patterns at $M = 4.0$ on Some Delta Wings. ARC R&M 3373, 1964.
- Squire, L. C.: Calculations of the Pressure Distribution on Lifting Conical Wings With Applications to the Off-Design Behaviour of Wave-Riders. AGARD CP-30, May 1968.
- Squire, L. C.: Flow Regimes Over Delta Wings at Supersonic and Hypersonic Speeds. Aeron. Quart., vol. 27, Feb. 1976, pp. 1-14.
- Squire, L. C.: The Independence of Upper and Lower Wing Flows at Supersonic Speeds. Aeronaut. J., paper 389, Oct. 1976, pp. 452-456.
- Squire, L. C.; Jones, J. G.; and Stanbrook, A.: An Experimental Investigation of the Characteristics of Some Plane and Cambered 65° Delta Wings at Mach Numbers from 0.7 to 2.0. ARC R&M 3305, 1961.
- Stahl, W. H.: Aerodynamics of Low Aspect Ratio Wings. AGARD-LS-98, Feb. 1979.
- Stanbrook, A. and Squire, L. C.: Possible Types of Flow at Swept Leading Edges. Aeronaut. Quart., vol. XV, 1964, pp. 72-82.

Stallings, R. L.; Burbank, P. B.; and Howell, D. T.: Heat Transfer and Pressure Measurements on Delta Wings at Mach Numbers of 3.51 and 4.65 and Angles of Attack from -45° to 45° . NASA TN D-2387, Aug. 1964.

Szodruch, J.: Lee Side Flow Fields of Delta Wings With Detached Shock Waves. Euromech 74 Colloquium, Cambridge/England, April 1976.

 Szodruch, J.: Leeseiten-Strömung bei schlanken Deltaflügeln endlicher Dicke (Lee Side Flow Over Slender Delta Wings with Large Thickness-to-Chord Ratio). ILR Bericht 23, Techn. Univ. Berlin, 1977.

Szodruch, J.: Reynolds Number Influence on Lee Side Flow Fields. AIAA Journal, vol. 16, no. 12, Dec. 1978, pp. 1306-1309.

Szodruch, J.: Zur Systematik der Leeseitenströmung bei Deltaflügeln (On the Systematics of Lee Side Flow Over Delta Wings). Zeitschrift für Flugwissenschaften, Band 4, Heft 2, 1980.

Szodruch, J.; and Ganzer, U.: On the Lee Side Flow Over Delta Wings at High Angles of Attack. AGARD CP 247, 1978.

Szodruch, J.; and Squire, L. C.: Pressure Distribution on the Suction Surfaces of Some Delta Wings at $M = 3.5$. ARC 35008, FM 4442, Hyp. 956, 1974.

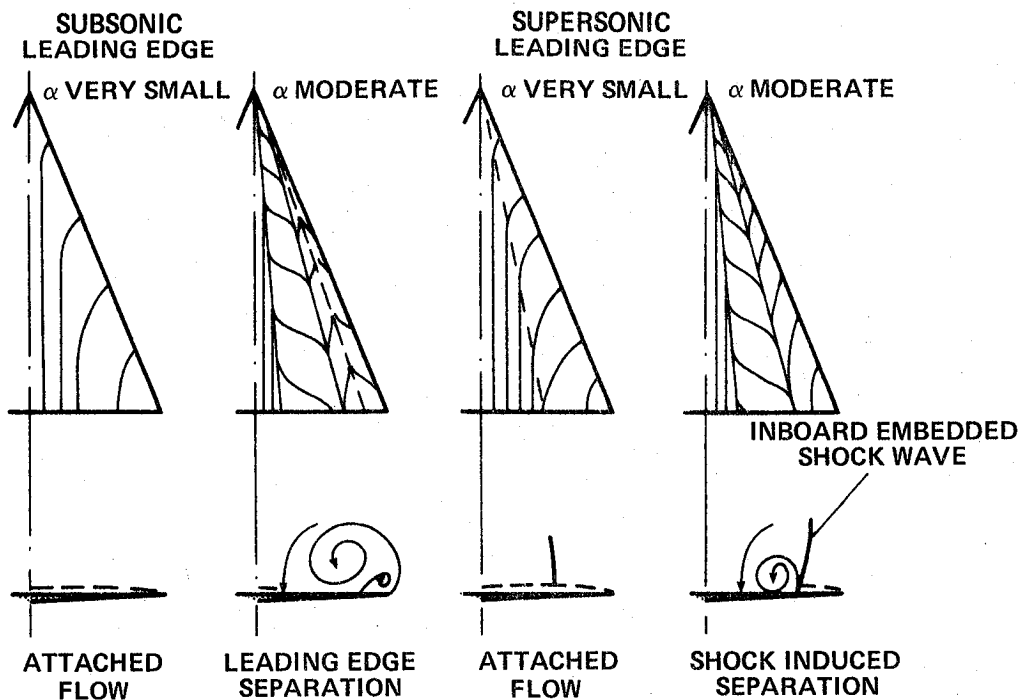
Thomann, H.: Measurements of Heat Transfer, Recovery Temperature and Pressure Distribution on Delta Wings at $M = 3.0$. FAA rep. 93, Stockholm, Sweden, 1963.

Tobak, M.; and Peake, D. J.: Topology of Two-Dimensional and Three-Dimensional Separated Flows. AIAA Paper 79-1480, July 1979.

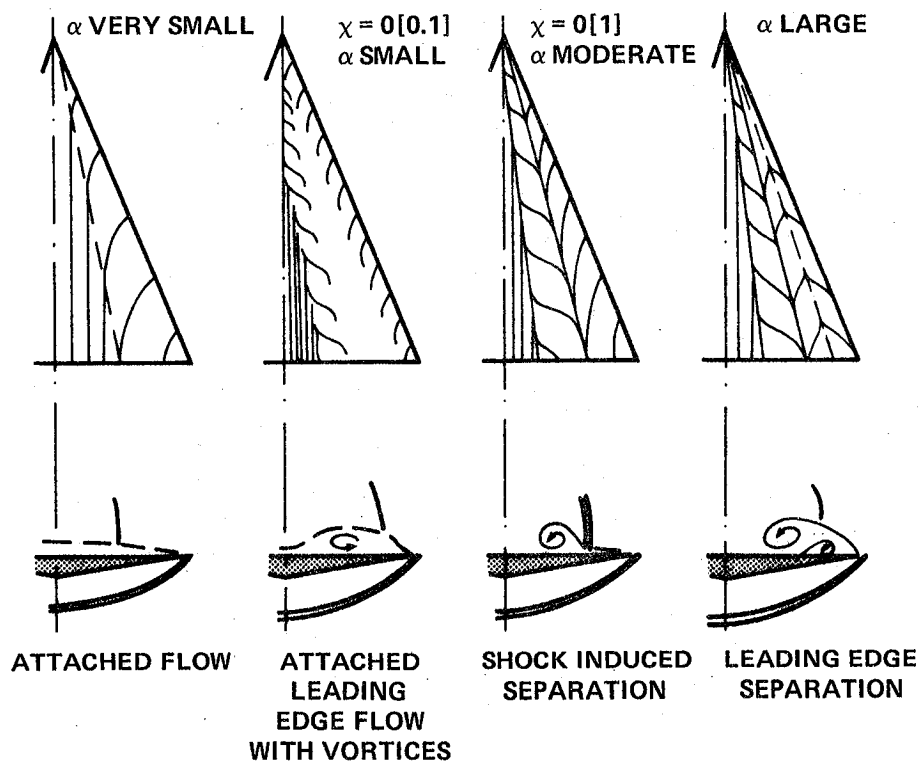
Vigneron, Y. C.; Rakich, J. V.; and Tannehill, J. C.: Calculation of Supersonic Viscous Flow Over Delta Wings with Sharp Subsonic Leading Edges. AIAA Paper 78-1137, July 1978.

Voskresensky, G. P.: Numerical Study of the Supersonic Flow Around Wings. ICAS Proceedings 1978, vol. 1, B2-04.

Walkden, E.; Laws, G. T.; and Caine, P.: Shock Capturing Numerical Method for Calculating Supersonic Flows. AIAA Journal, vol. 12, no. 5, May 1974, pp. 642-647.



(a) Stanbrook-Squire, supersonic speeds (1964).



(b) Narayan, hypersonic speeds (1978).

Figure 1.- Flow models.

REFERENCES	MODEL PARAMETER											EXPERIMENTAL PARAMETER														
	SWEEP				REL. HEIGHT				UPPER SURFACE SHAPE			RE NUMBER	L.E. TYPE		MACH NUMBER			SHOCK TYPE		ANGLE OF ATTACK						
	Λ , deg				t/L				FLAT	DELTA	CONE	$R_{L\infty}$	SHARP	BLUNT	M_∞			ATTACHED	DETACHED	α , deg						
	50	60	70	80	0	0.1	0.2	0.3							1	3	5			0	10	20	30	40		
LEE, 1955		■	■	■	■				■			0.5→12×10 ⁶	■		■	■		■			■					
FELLOWS + CARTER, 1969				■	■	■			■				■			■	■				■					
GREENWOOD, 1968			■					■		■		3.0×10 ⁶	■			■				■			■			
EDWARDS, 1965				■				■		■		20×10 ⁶	■	■			■				■			■		
DROUGGE + LARSON, 1956				■				■		■			■	■		■				■		■				
THOMANN, 1963		■	■	■				■		■		2×10 ⁶		■			■			■		■				
MONNERIE + WERLÉ, 1968				■				■		■		1→4.5×10 ⁶	■			■		■	■	■			■			
BANNIK + NEBBELINK, 1971	■							■		■		2.6×10 ⁶	■				■		■				■			
SQUIRE, 1963/1964				■	■					■	■	8.7×10 ⁶	■					■			■		■			
MICHAEL, 1955		■		■		■		■		■		14×10 ⁶	■			■				■		■				
MURRAY/STALLINGS, 1966			■		■			■		■		5→16×10 ⁶	■	■			■		■			■				
BASHKIN, 1967			■		■			■		■									■	■		■				
STALLINGS, et al., 1964				■				■		■		6.6×10 ⁶		■				■	■		■		■			
MORRIS + COUCH, 1968				■						0.5		4×10		■				■			■		■			
REIN, 1964		■						■		■		1.7×10 ⁶	■				■				■		■			
CRAVEN/ALEXANDER, 1963				■				■		■		0.6×10 ⁶	■				■			■		■				
RICHARDS, 1976				■				■		■		0.4×10 ⁶	■				■			■		■				
SZODRUCH, et al., 1974, 1977, 1978				■				■		■	■	0.7→7.6×10 ⁶	■				■				■		■			

Figure 2.- Parameters of lee side flow investigations at supersonic speeds.

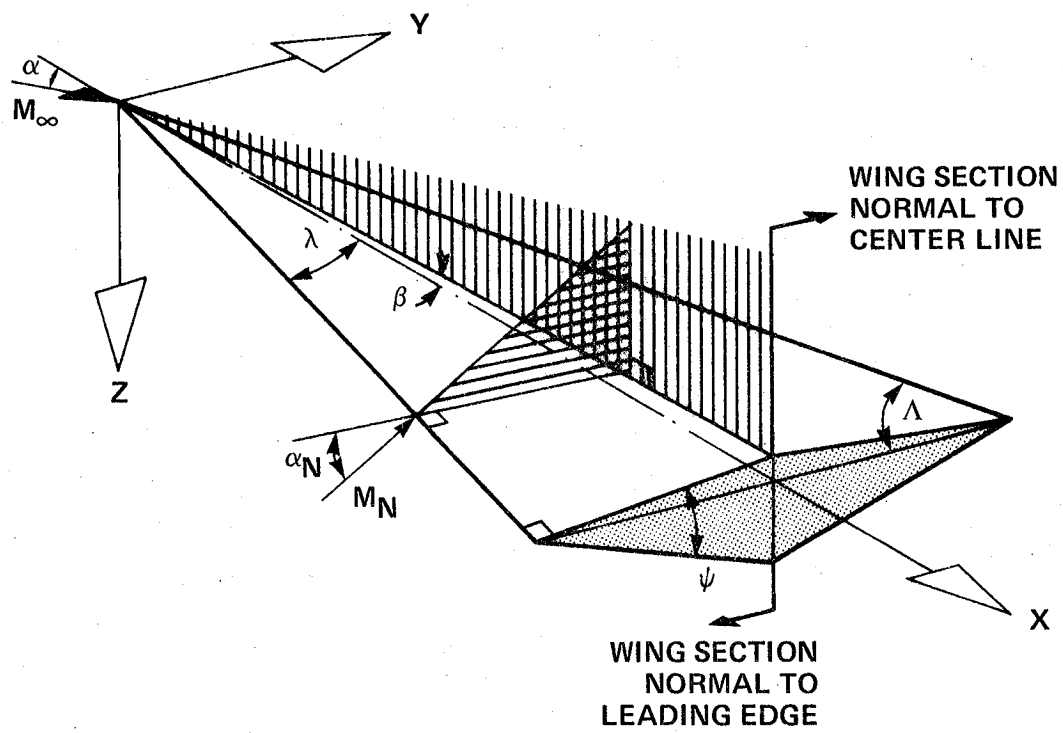
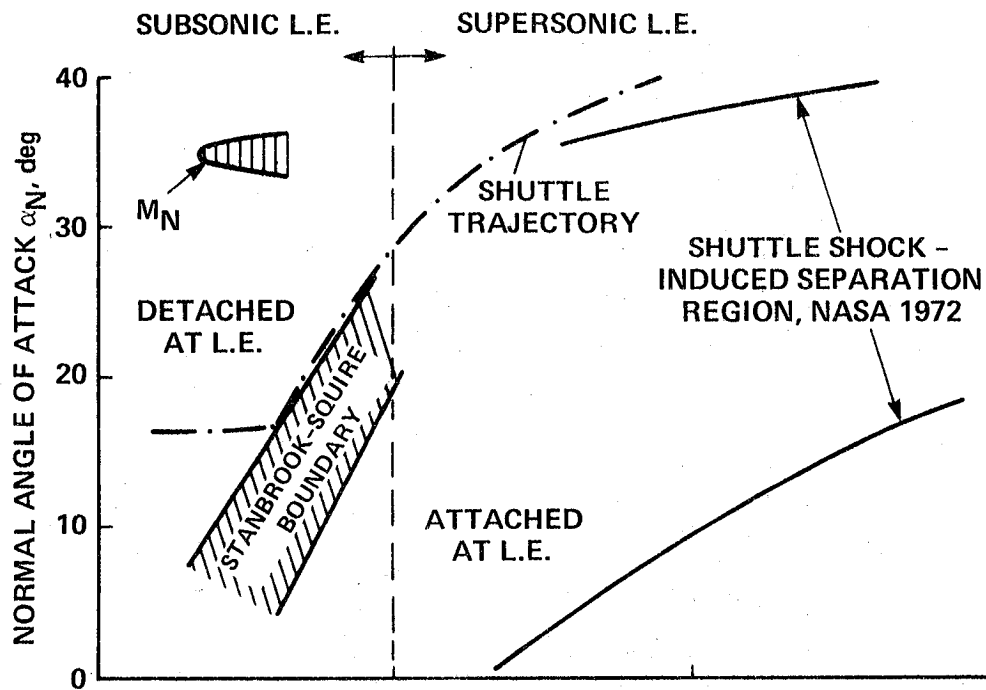
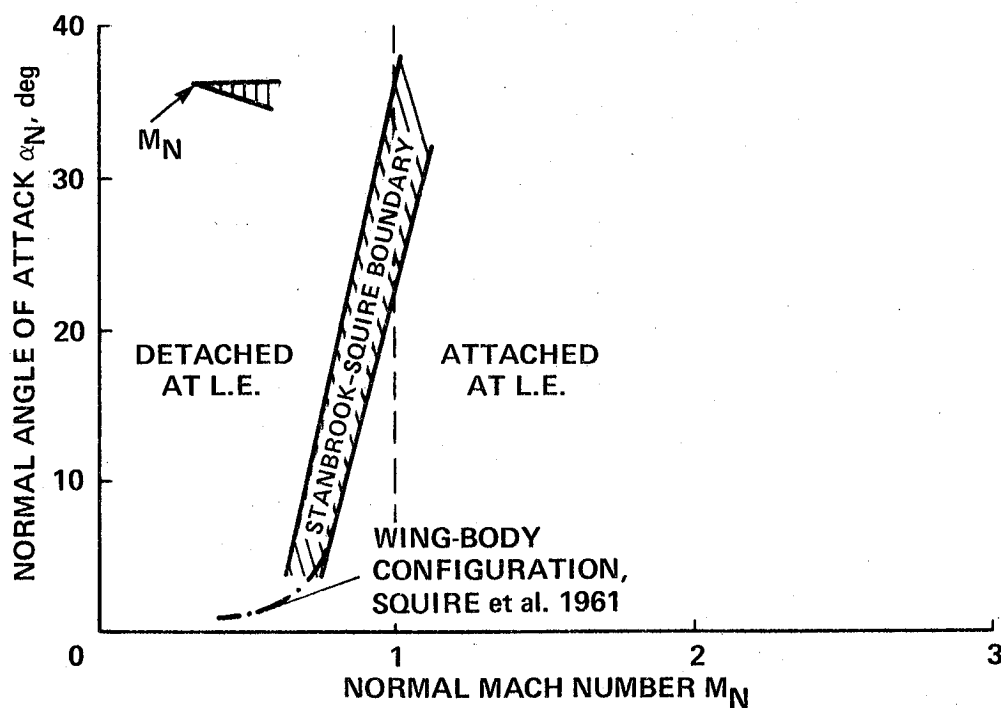


Figure 3.- Delta wing geometry and flow components.



a) ROUNDED LEADING EDGE



b) SHARP LEADING EDGE

Figure 4.- Detached and attached flow at swept leading edges (Stanbrook and Squire 1964).

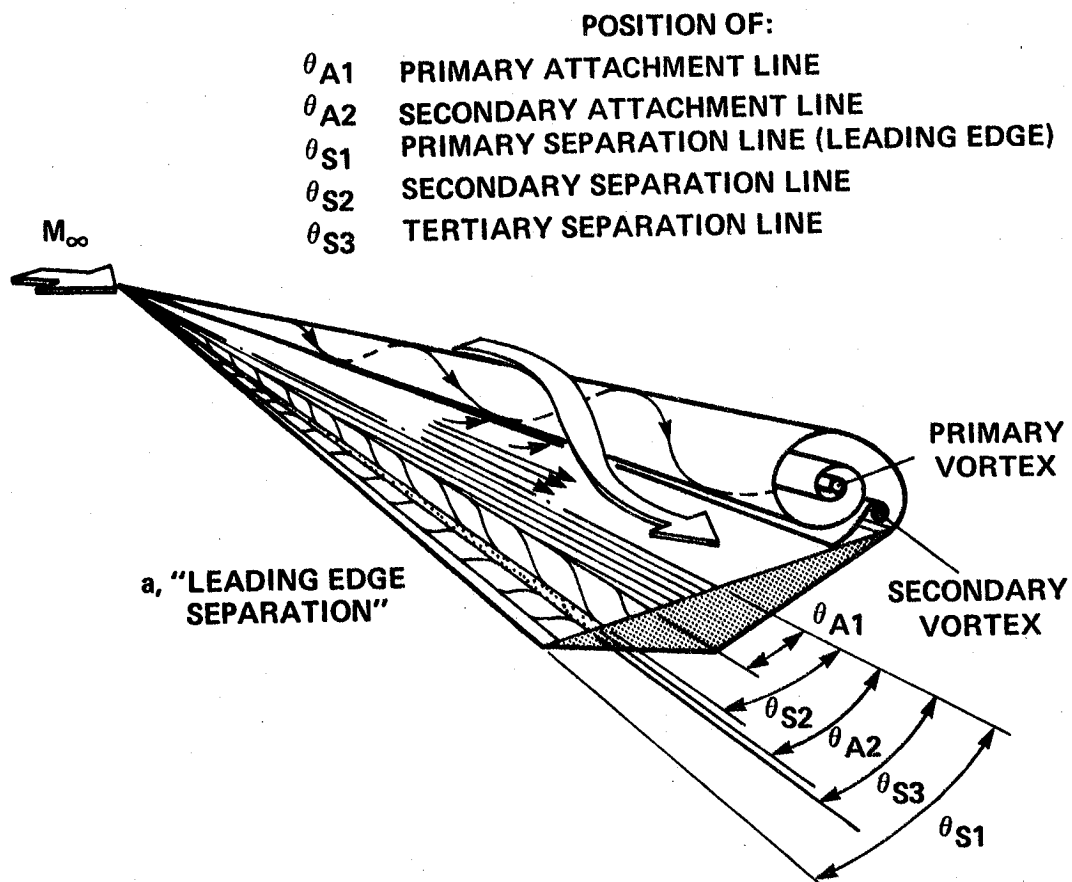


Figure 5.- Skin-friction line pattern and external flow structure about flat-topped delta wing.

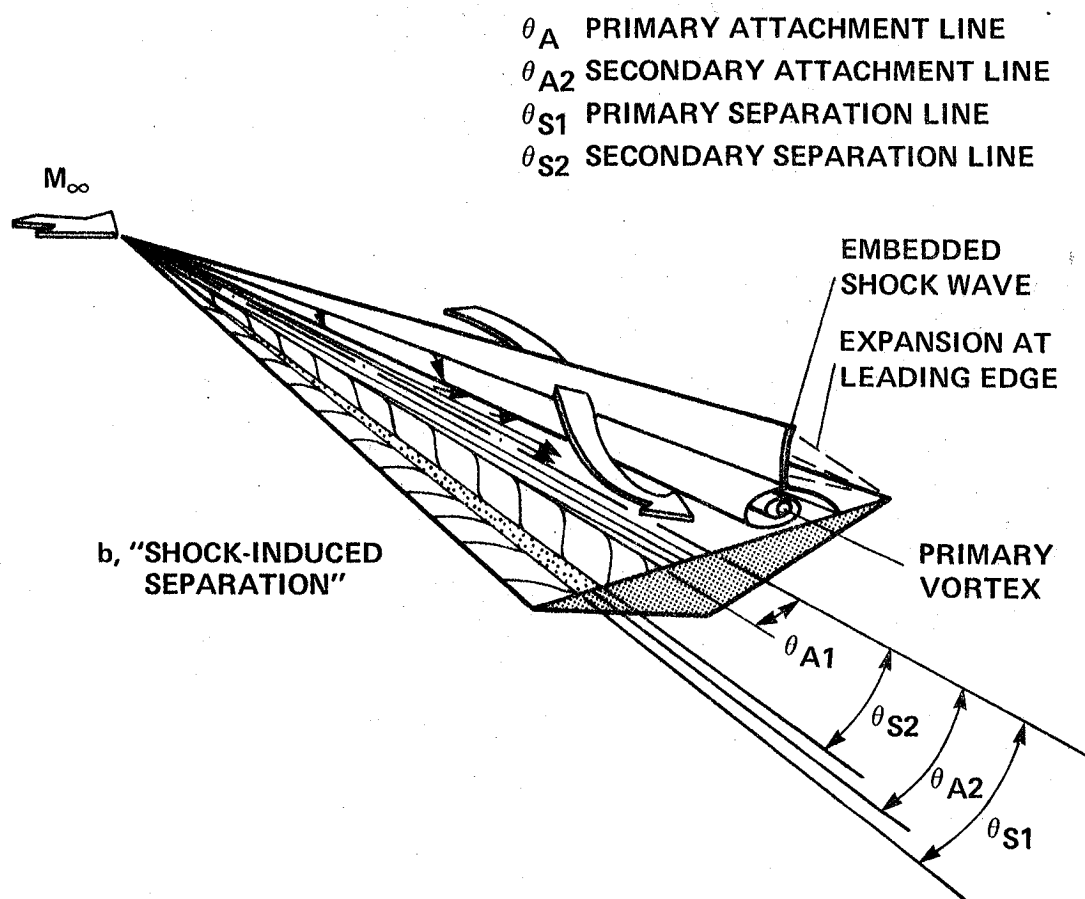
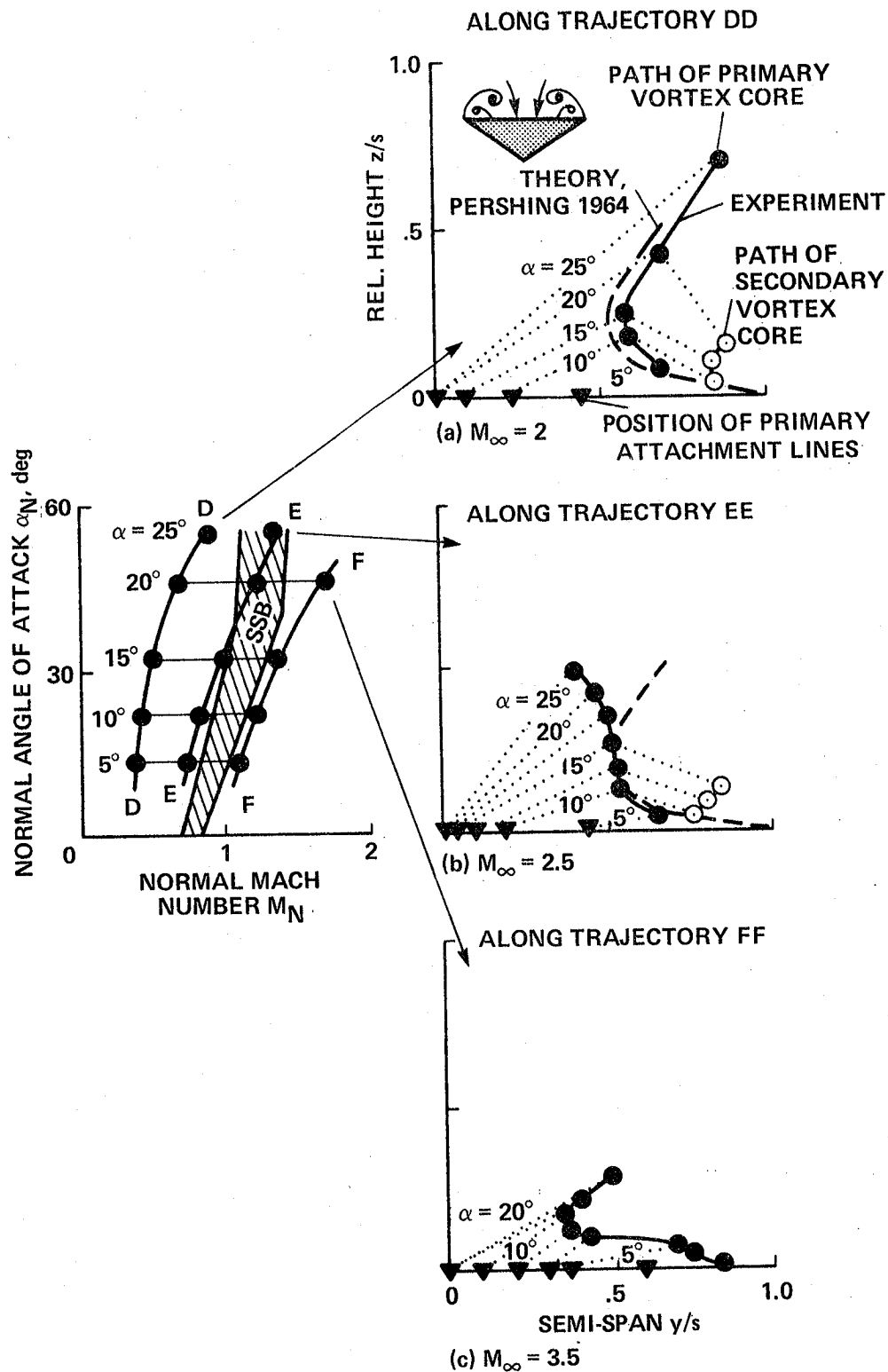


Figure 5.- Concluded.



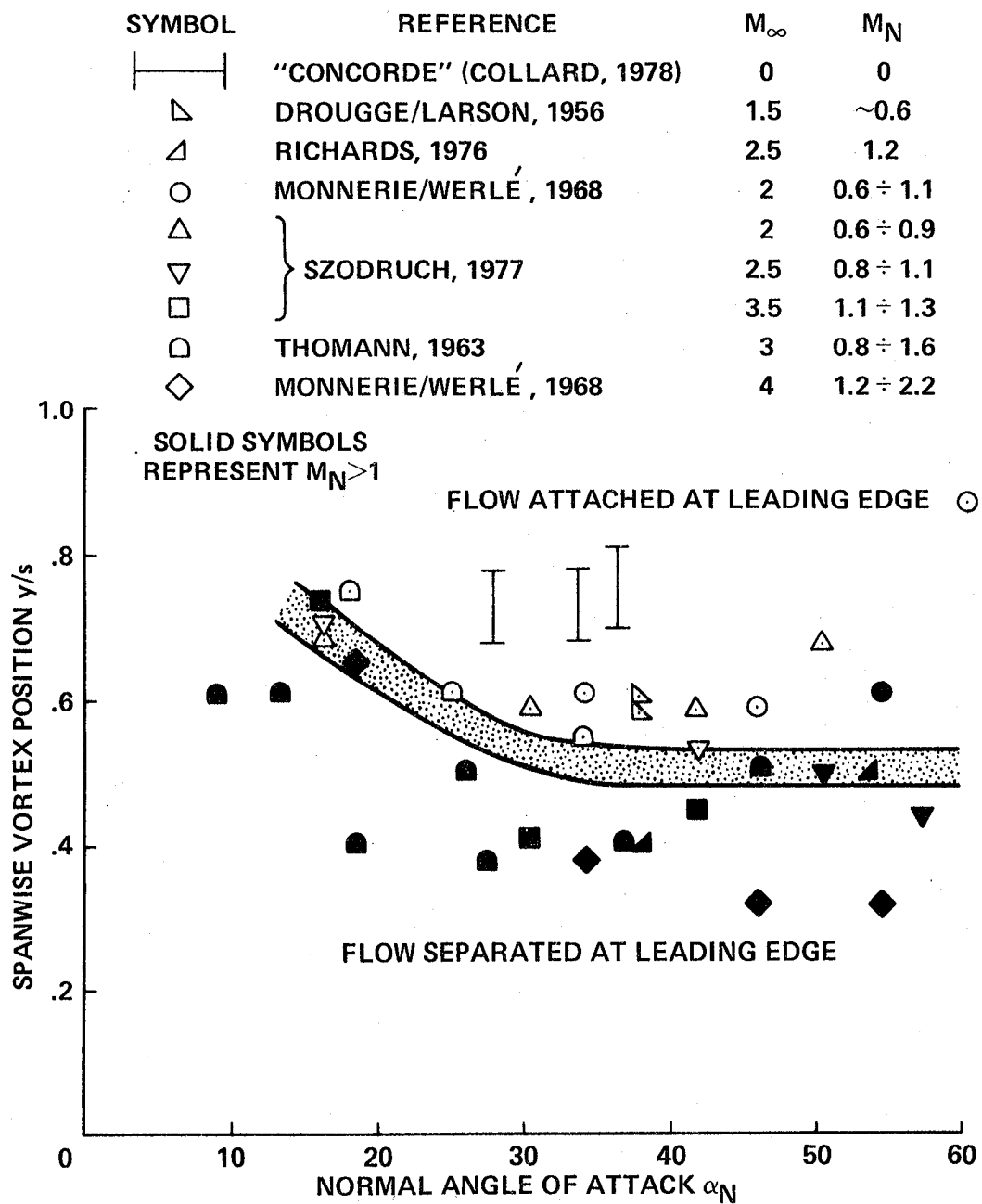


Figure 7.- Vortex position exhibiting certain types of delta wing flow.

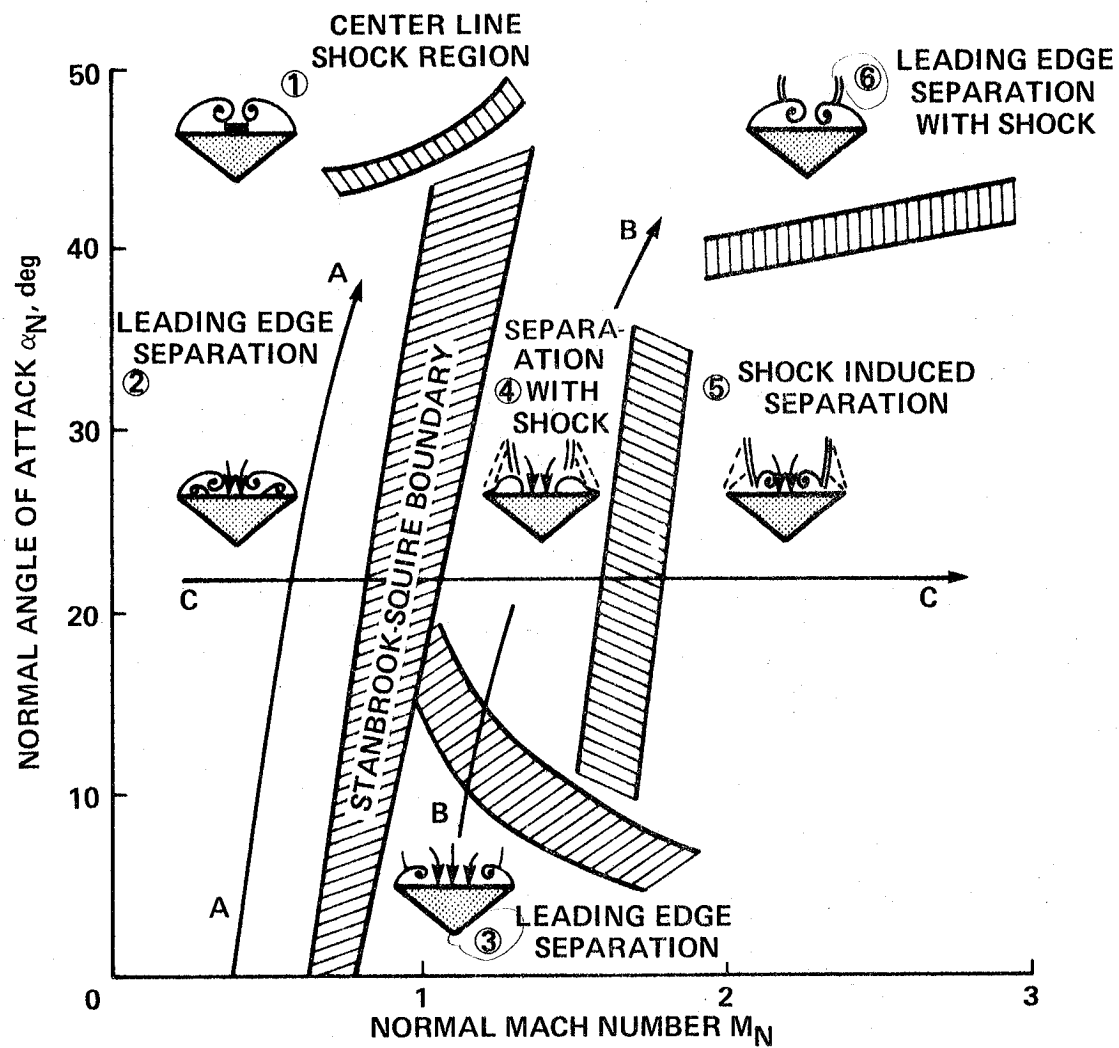
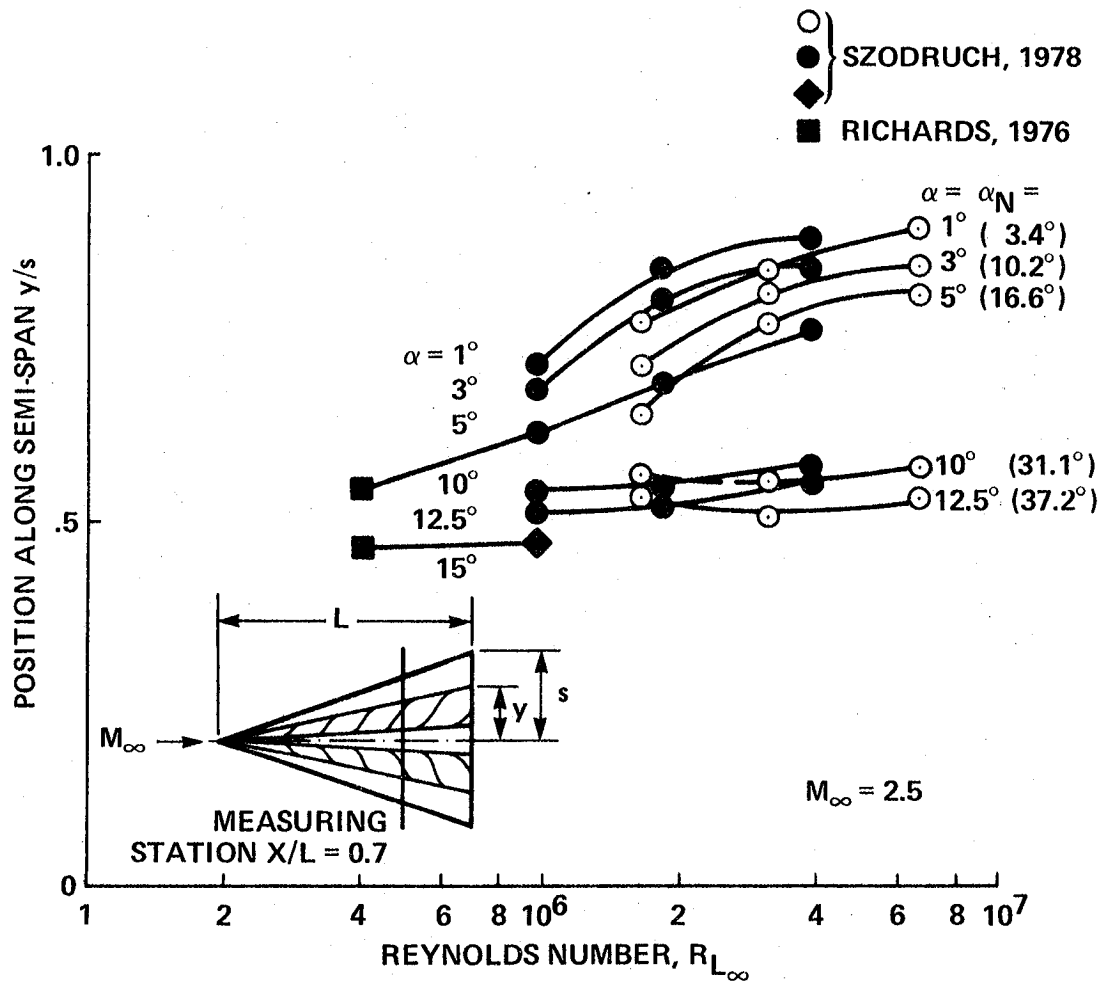
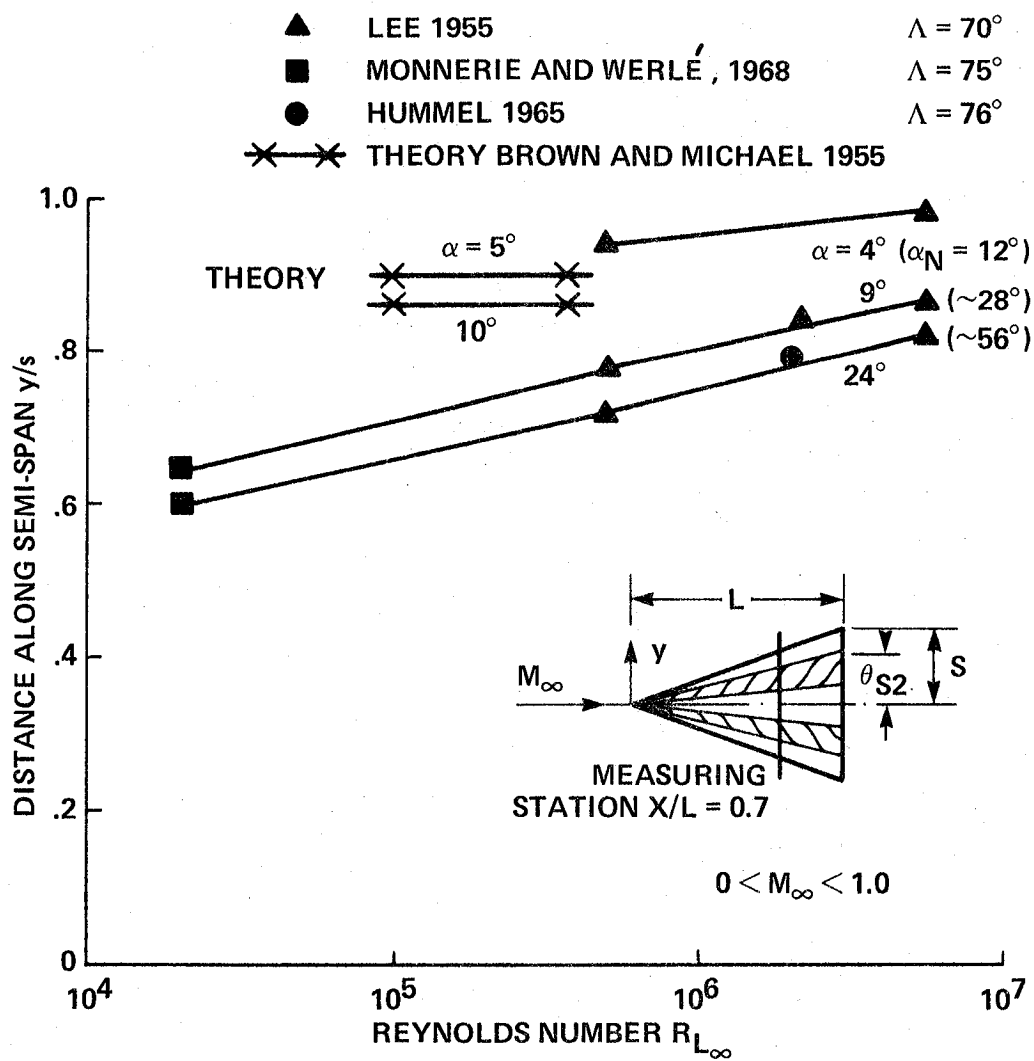


Figure 8.- Lee side flow regimes over thick delta wings at supersonic speeds - α_N vs M_N diagram (Szodruch, 1978).



(a) Supersonic Mach numbers.

Figure 9.- Influence of Reynolds number on skin-friction line pattern.



(b) Subsonic Mach numbers.

Figure 9.- Concluded.

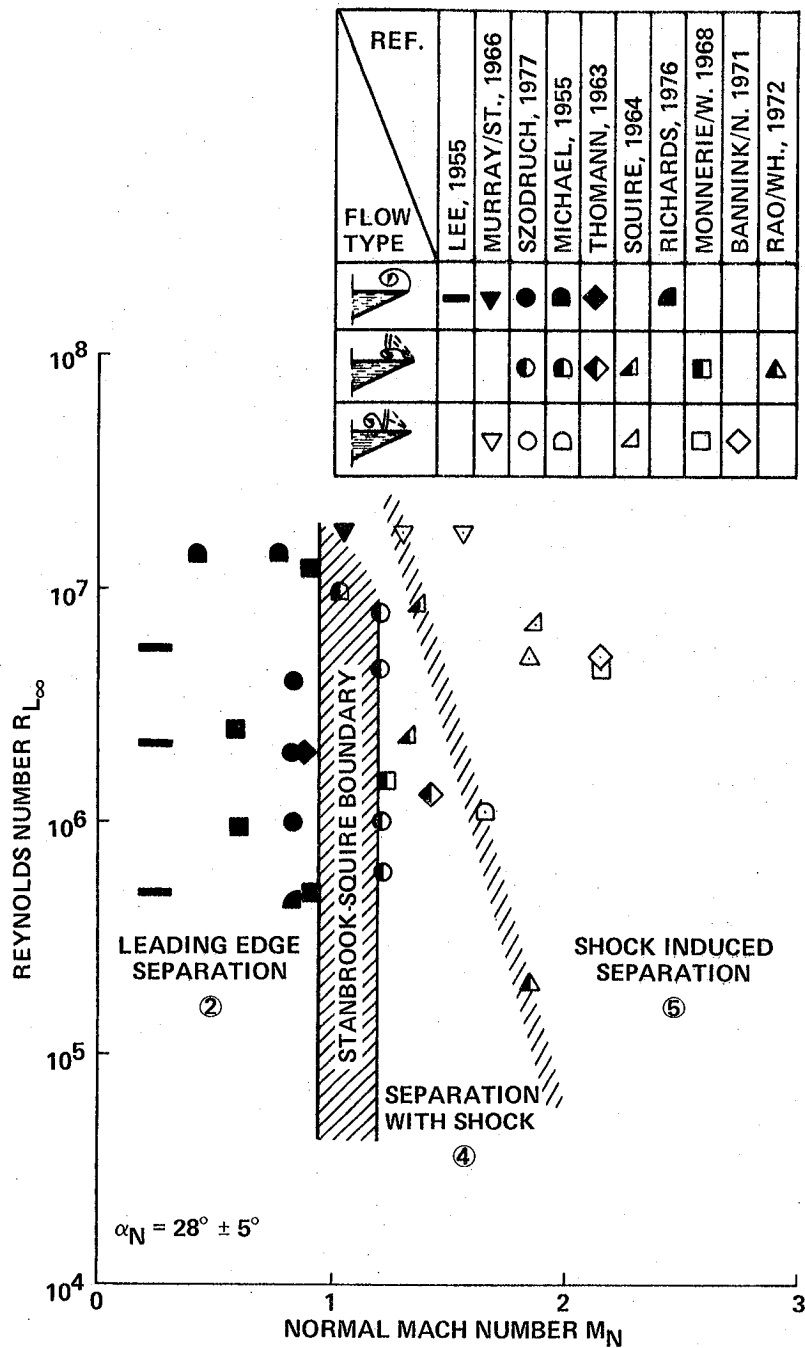


Figure 10.- Influence of Reynolds number on flow types and boundaries at constant α_N .

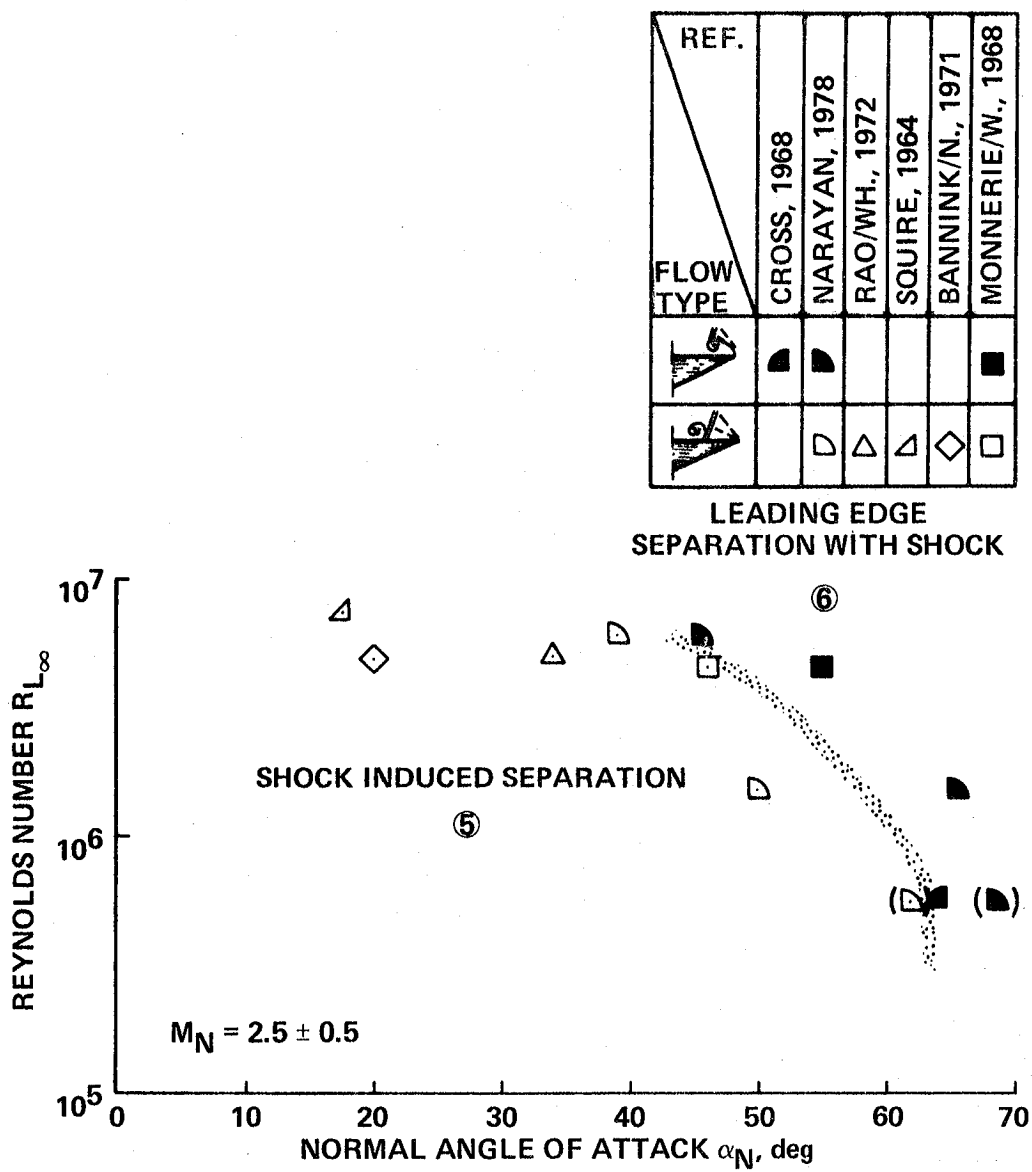
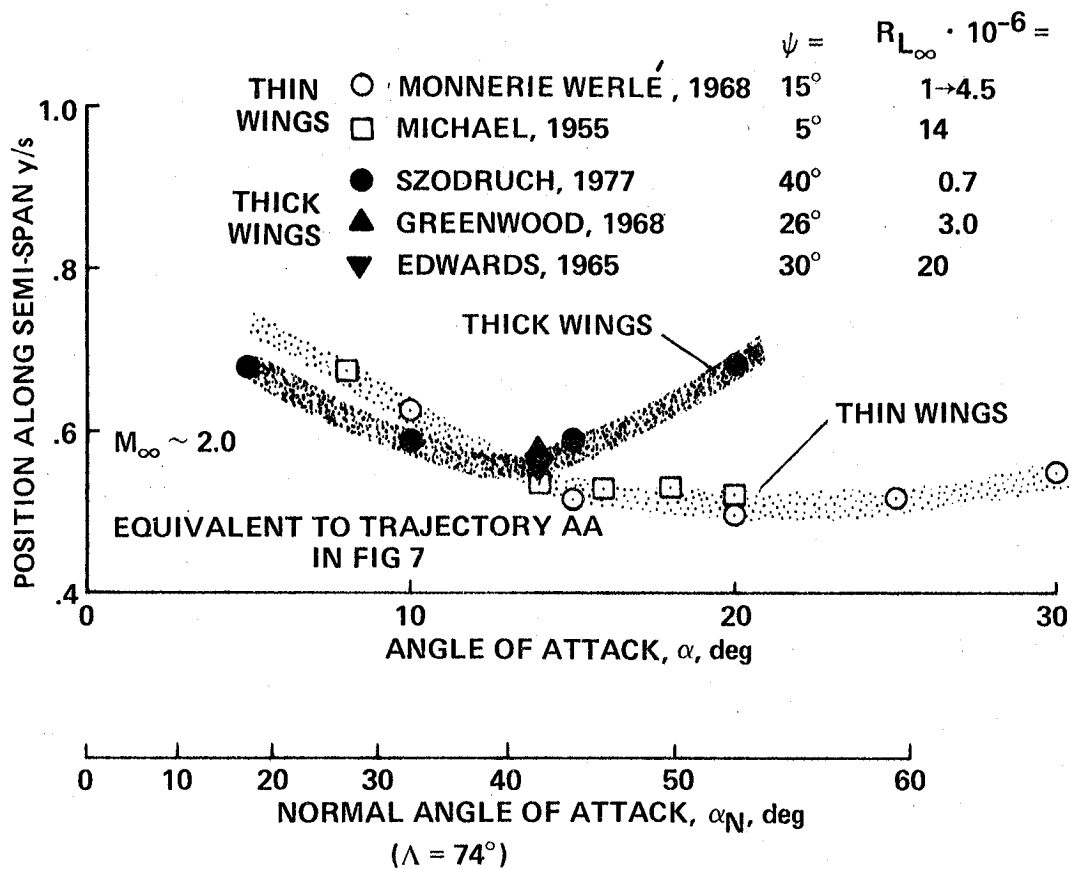
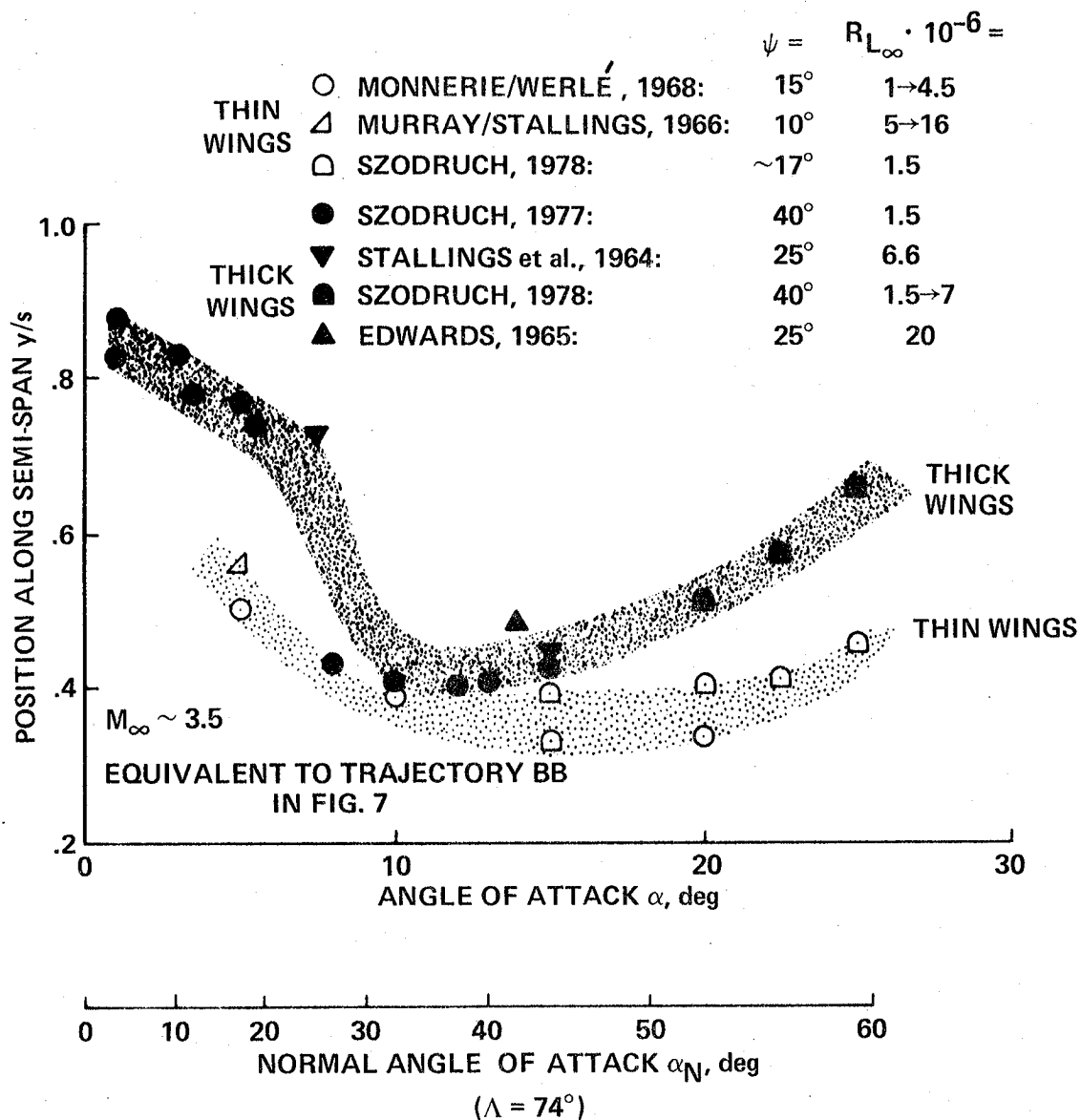


Figure 11.- Influence of Reynolds number on flow types and boundaries at constant M_N .



(a) Left-hand side of "Stanbrook-Squire Boundary" (region 2 in fig. 8).

Figure 12.- Secondary separation line positions for thick and thin wings.



(b) Right-hand side of "Stanbrook-Squire Boundary" (regions 3, 4, and 6 in fig. 8).

Figure 12.- Concluded.

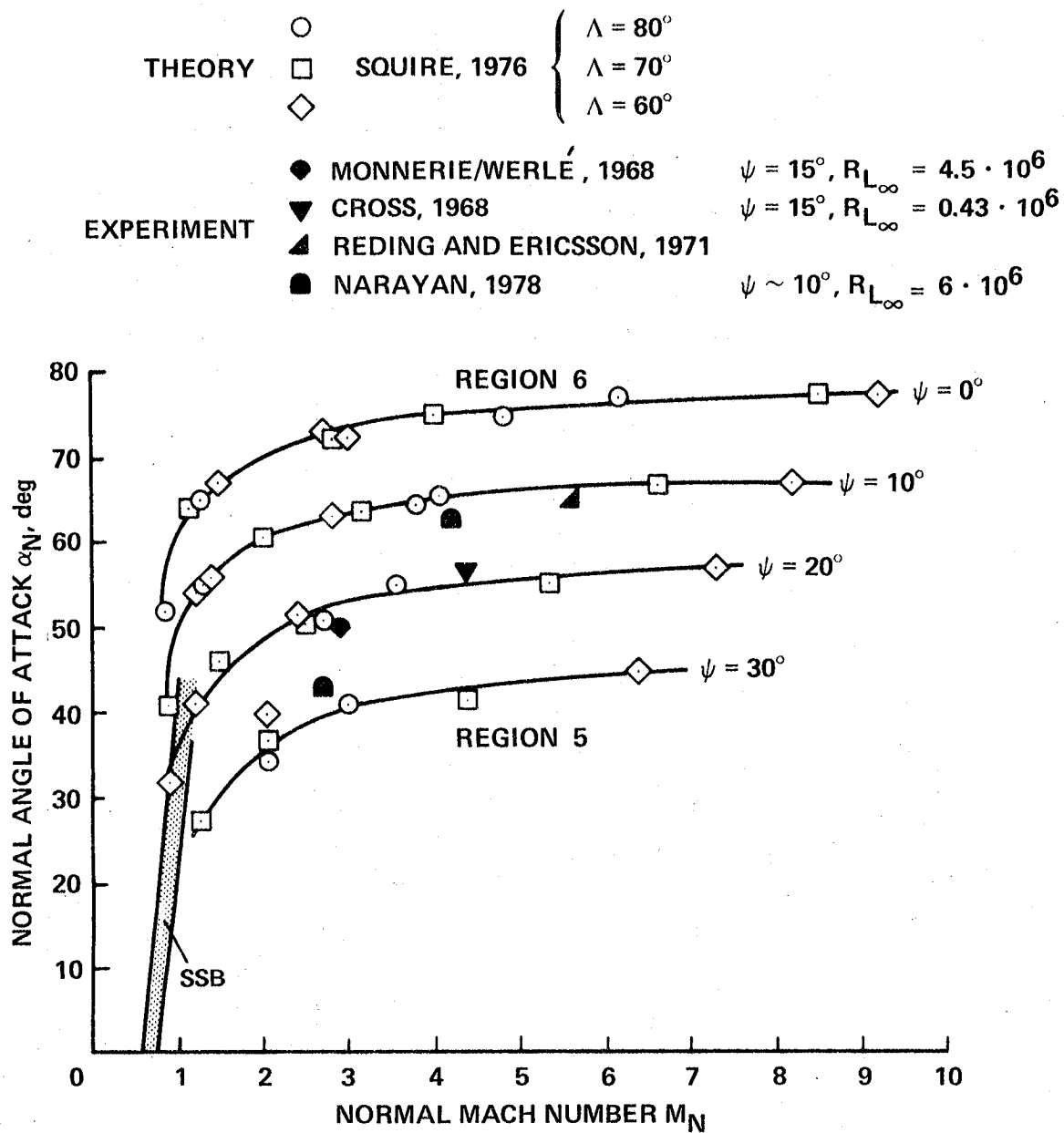


Figure 13.- Flow regions over thin and thick wings according to thin-shock-layer theory (Squire, 1976).

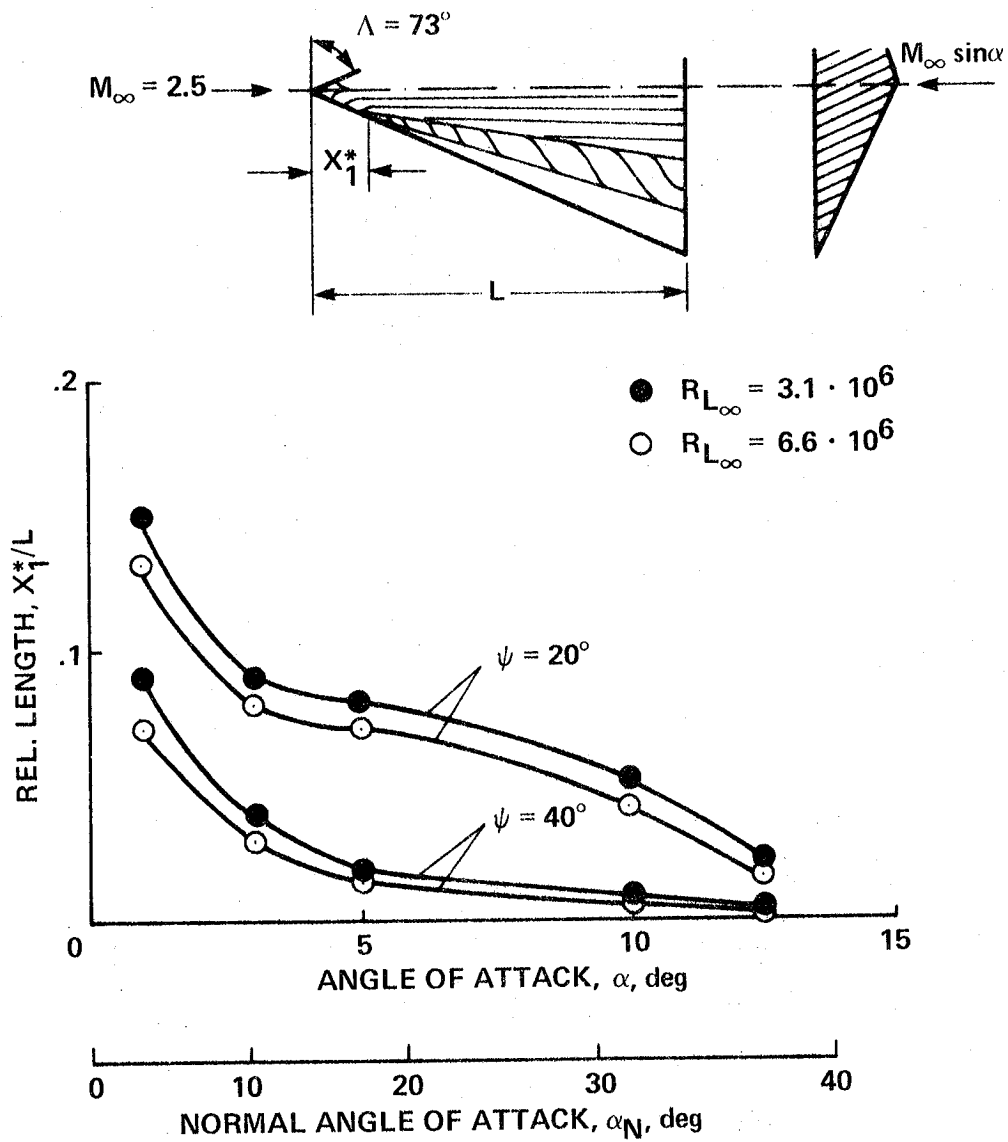


Figure 14.- Influence of Reynolds number and leading-edge angle ψ on visual start of leading-edge separation line.

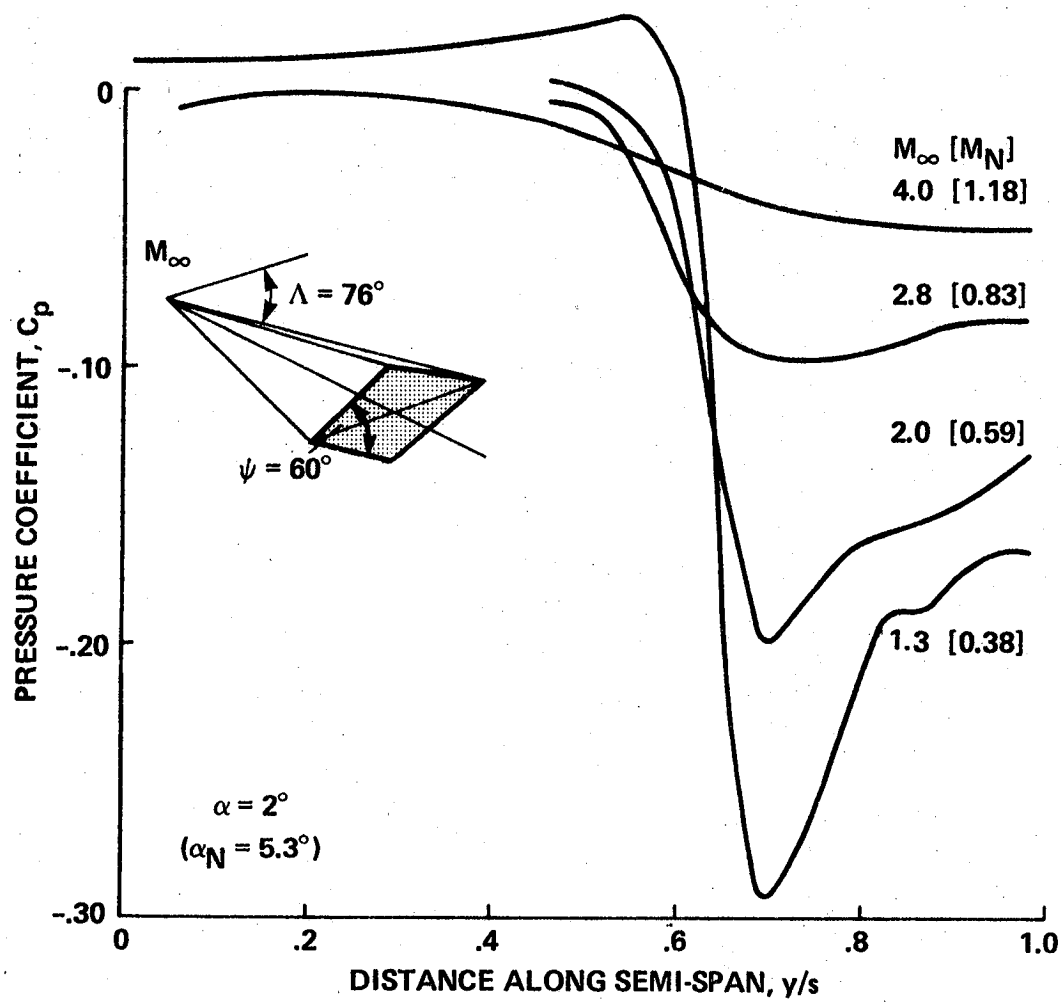


Figure 15.- Pressure distribution over a diamond-shaped delta wing at various Mach numbers (Küchemann, 1964).

BS = BOW SHOCK WAVE
A = PRIMARY ATTACHMENT LINE
S1 = LINE OF PRIMARY SEPARATION
S2 = LINE OF SECONDARY SEPARATION
P = VORTEX CENTER IN VERTICAL
DISTANCE FROM SCHLIEREN
EXPERIMENTS

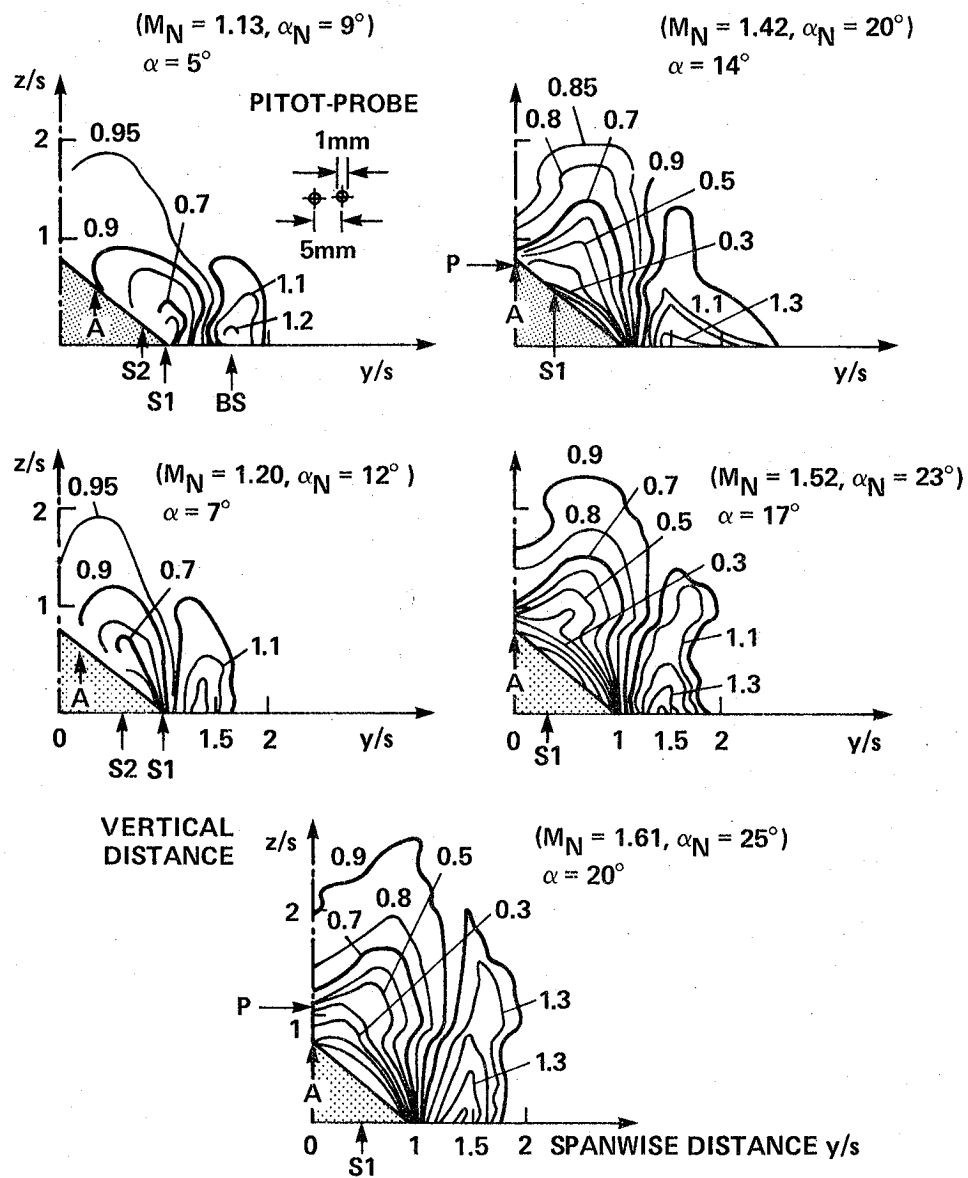


Figure 16.- Contours of constant pitot pressure (P_p/P_{p_∞}) in the leeward flow field of a delta wing with flat underside ($\beta = 14.5^\circ$) at $M_\infty = 2.6$ and $R_{L_\infty} = 0.7 \times 10^6$ (Szodrach, 1977).

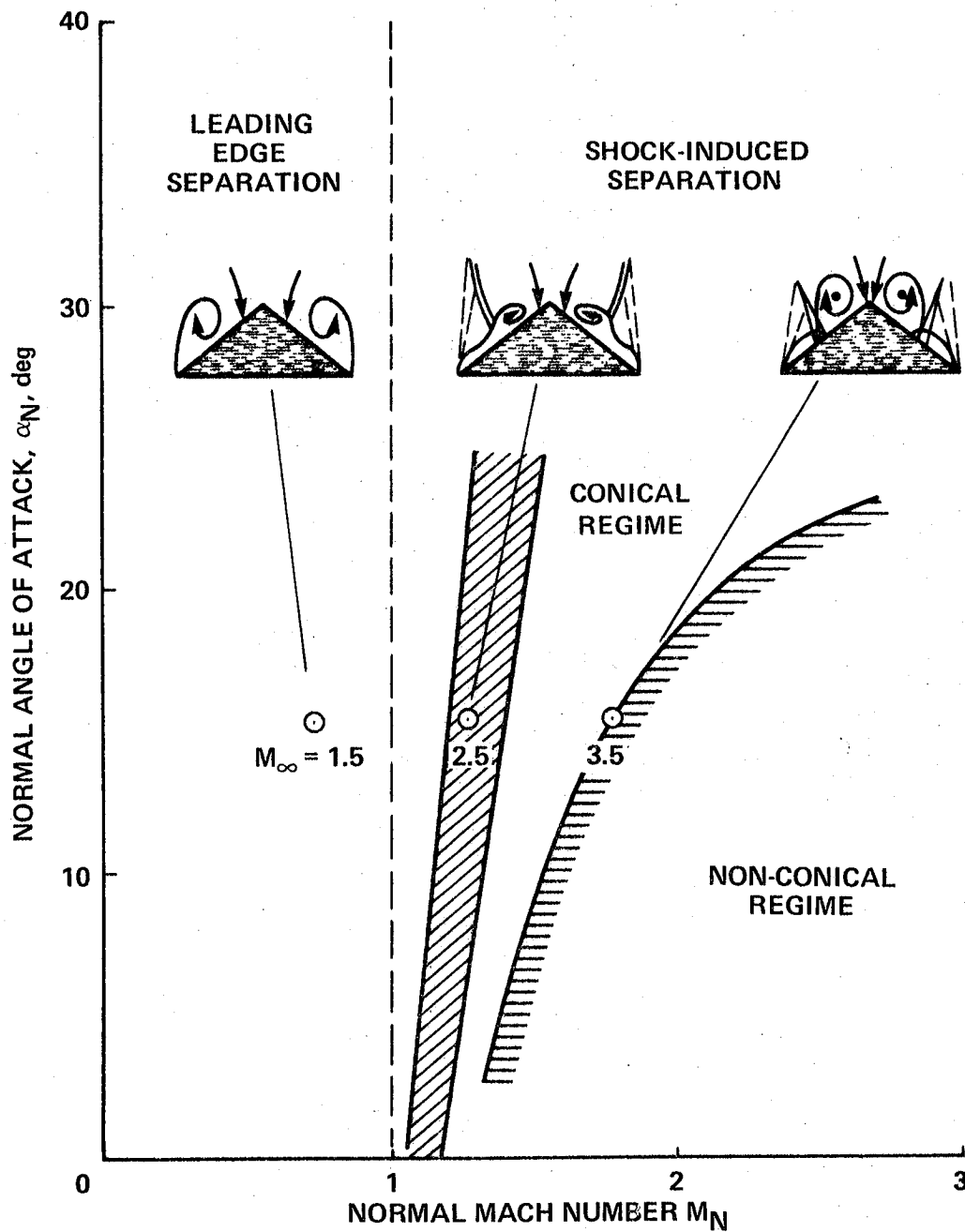


Figure 17.- Leeward flow regimes over thick delta wings ($\beta = 14.5^\circ$) with flat underside (Szodruch, 1980).

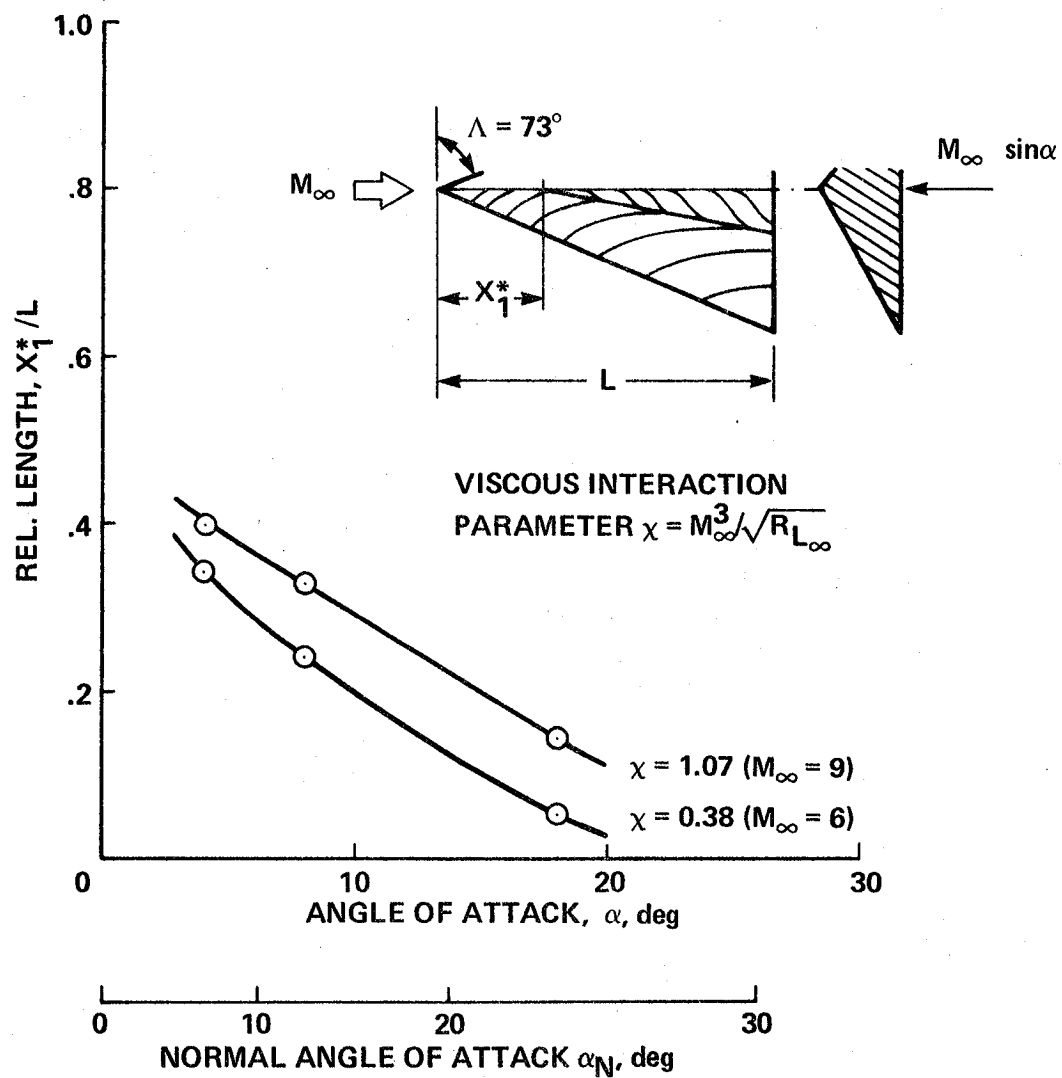


Figure 18.- Influence of viscous interaction parameter χ on the visual start of the inboard separation line for a thick wing ($\beta = 14.5^\circ$) with flat underside (Szodruch, 1980).

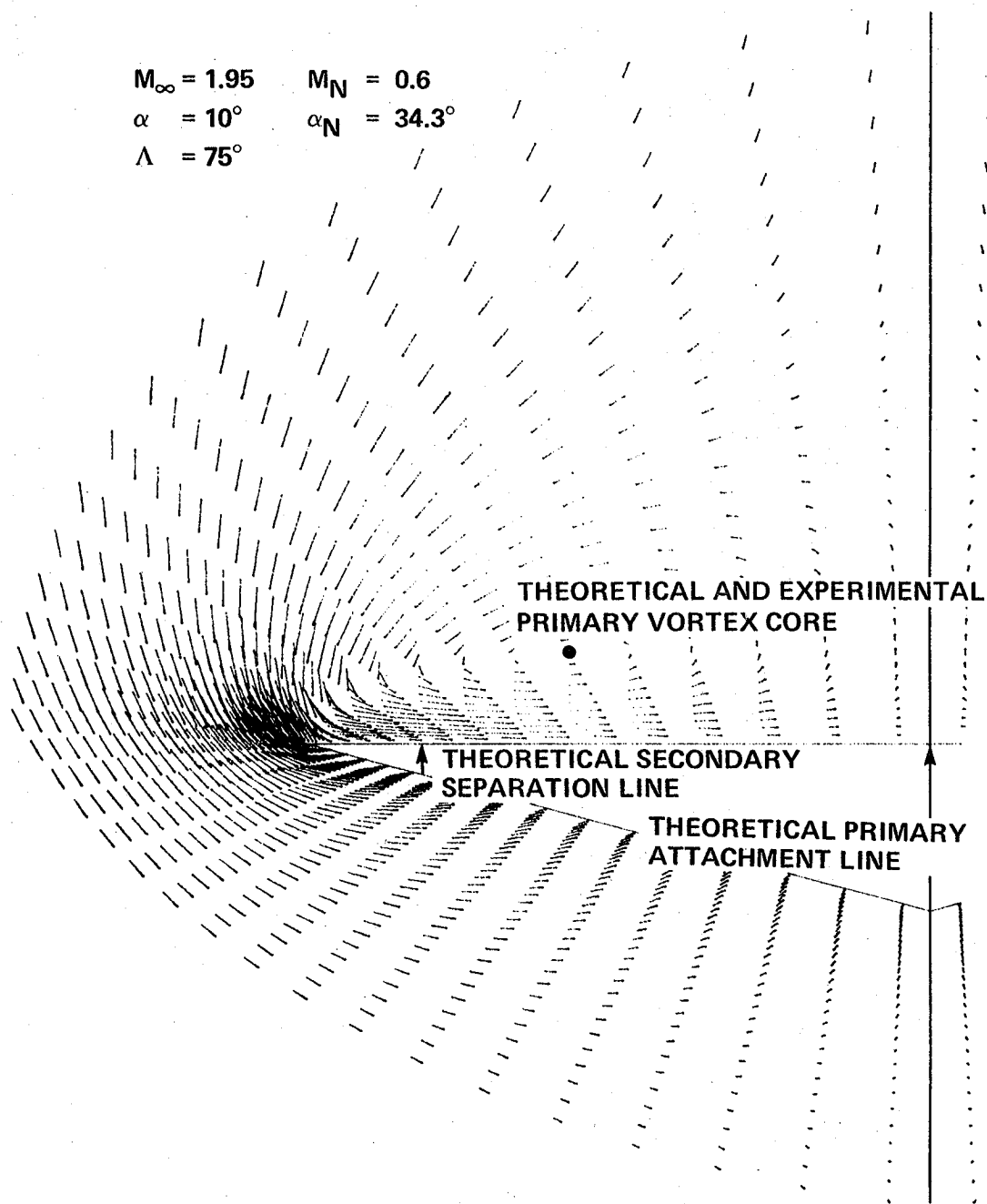


Figure 19.- Crossflow velocities around delta wing ($\psi = 15^\circ$) at supersonic speed with leading-edge separation, $R_{L_{\infty}} = 10^6$ (Vigneron, et al., 1978).

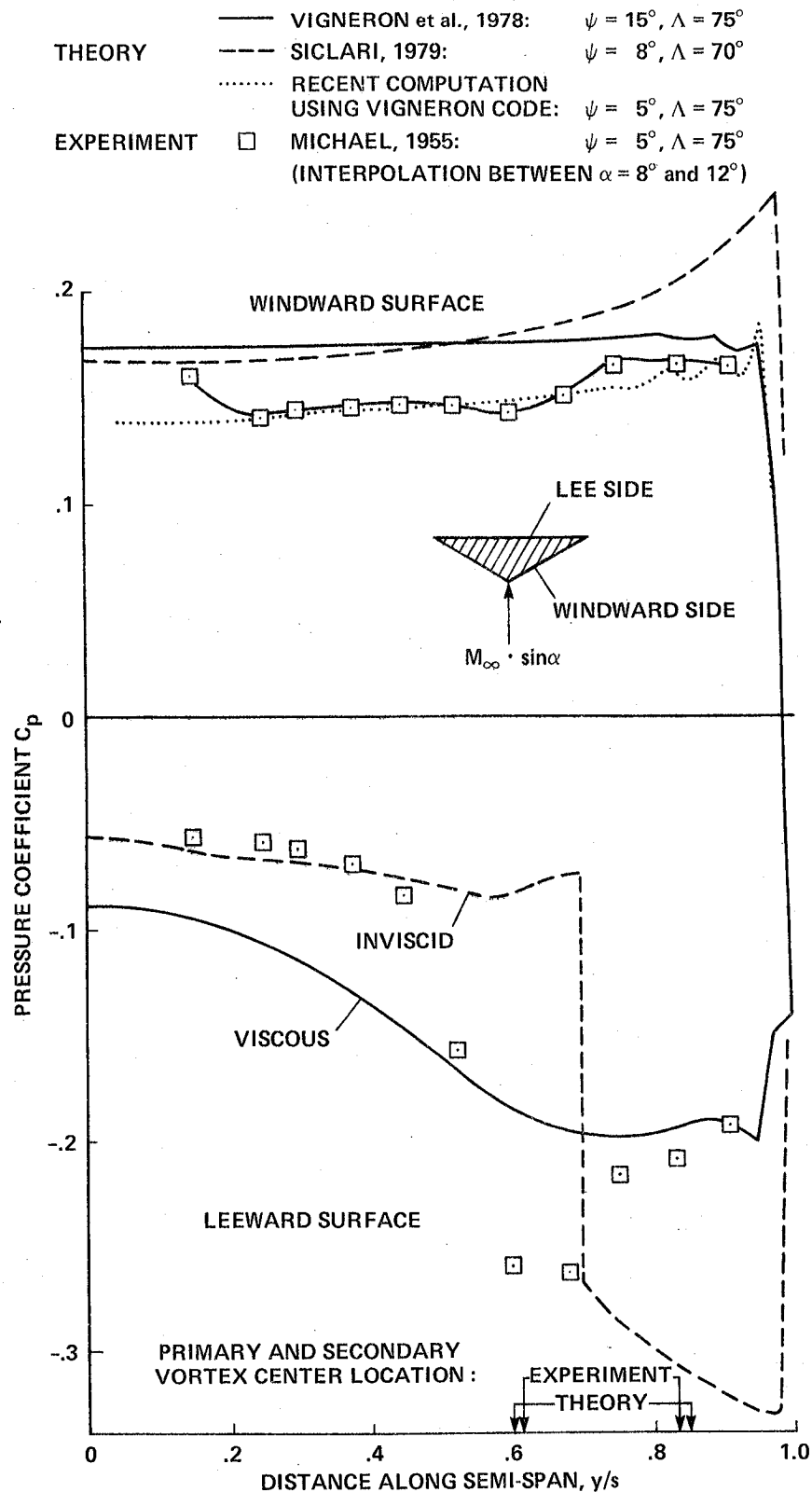


Figure 20.- Theoretical and experimental pressure distributions, $M_\infty = 2$ and $\alpha = 10^\circ$.

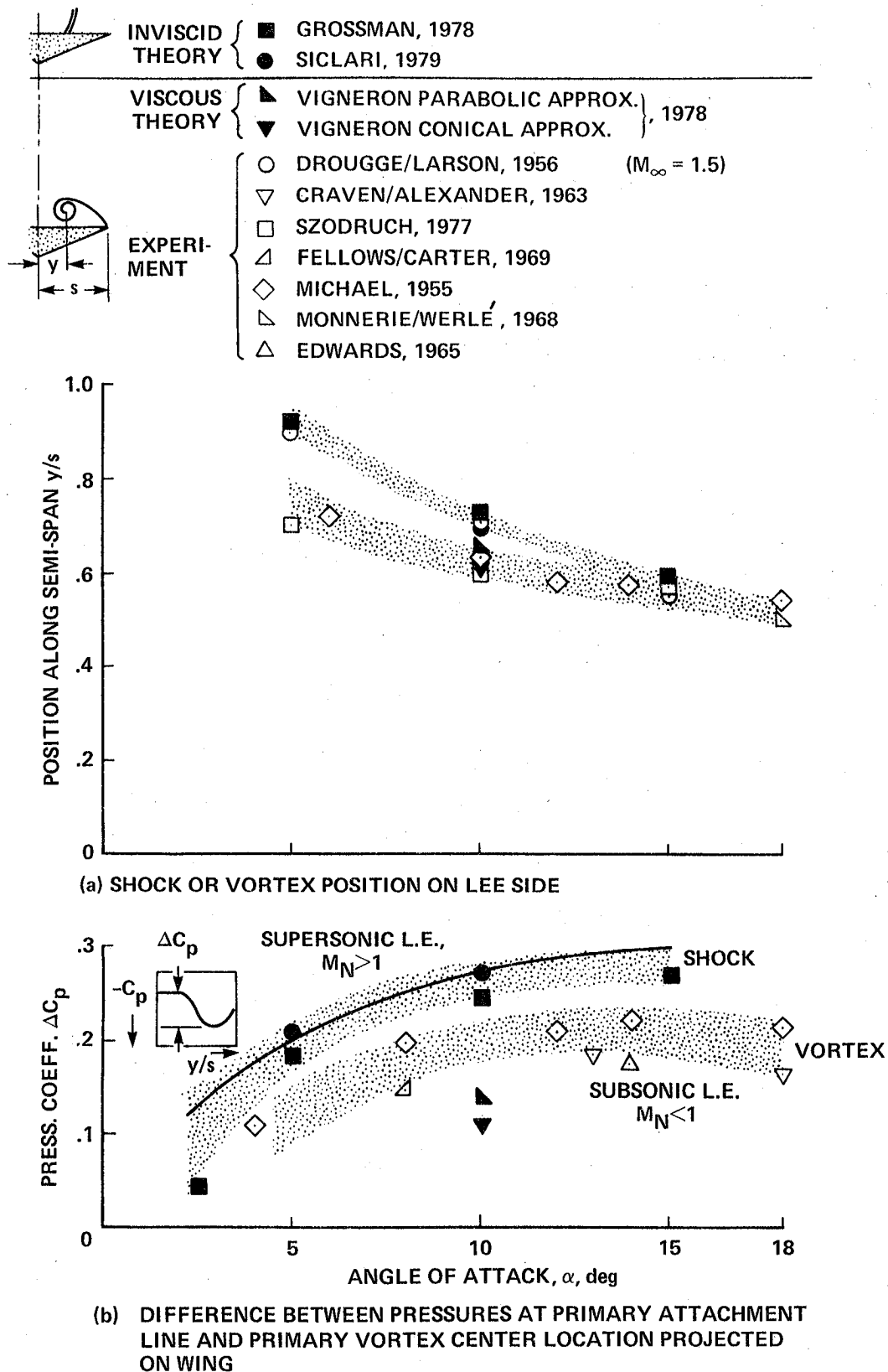
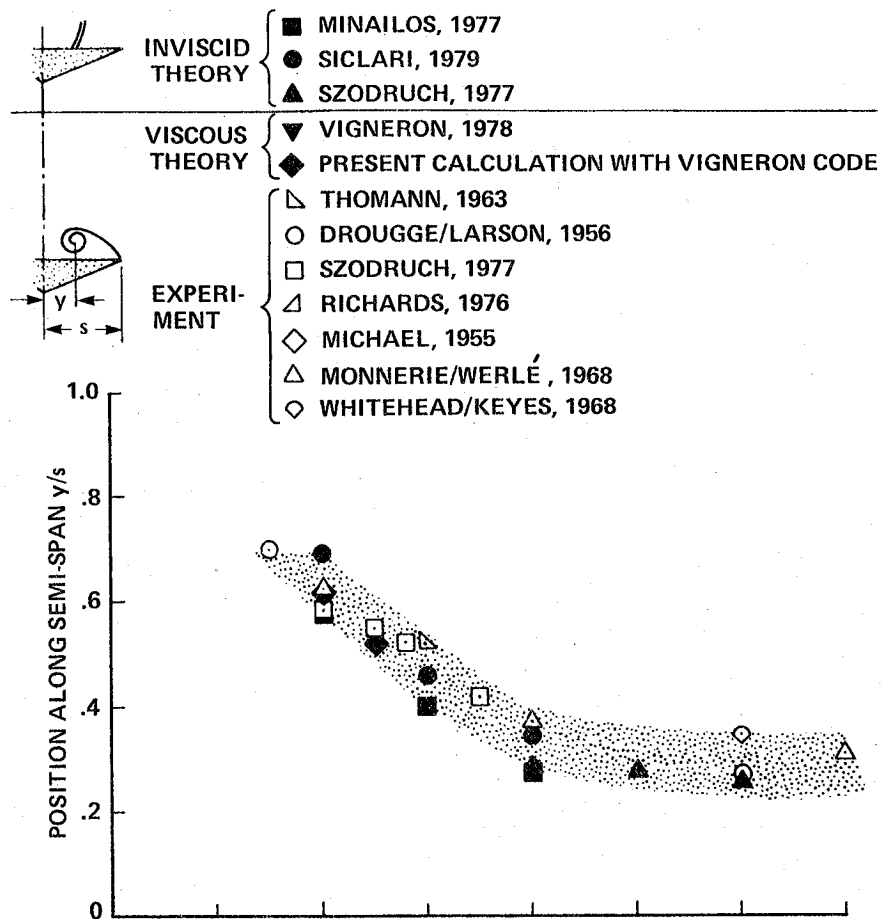
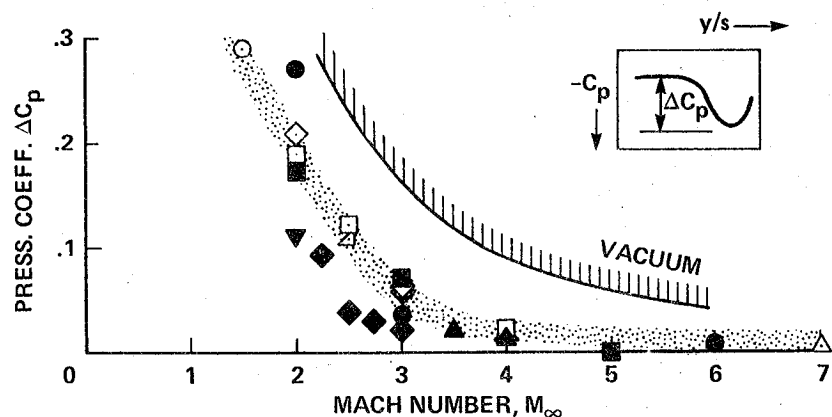


Figure 21.- Influence of angle of attack on theoretical and experimental lee side results, $M_\infty = 2$ and $\Lambda \sim 73^\circ$.



(a) SHOCK OR VORTEX POSITION ON LEE SIDE



(b) DIFFERENCE BETWEEN PRESSURES AT PRIMARY ATTACHMENT LINE AND PRIMARY VORTEX CENTER LOCATION PROJECTED ON WING.

Figure 22.- Influence of Mach number on theoretical and experimental lee-side results, $\alpha \sim 10^\circ$ and $\Lambda \sim 73^\circ$.

$$\begin{array}{ll}
 M_{\infty} = 2.94 & M_N = 1.99 \\
 \alpha = 12^{\circ} & \alpha_N = 16.7^{\circ} \\
 \Lambda = 45^{\circ} &
 \end{array}$$

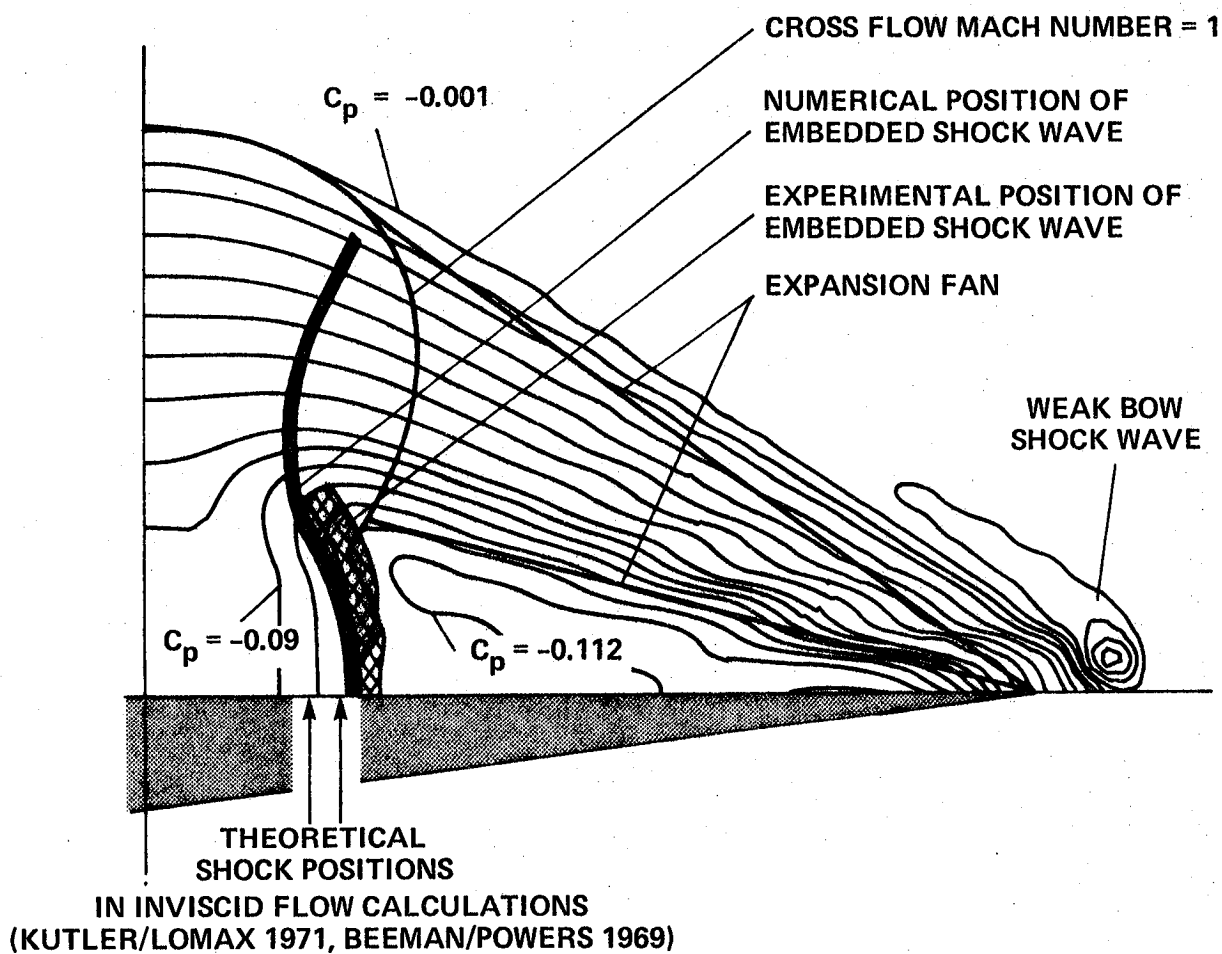


Figure 23.- Static pressure contours in crossflow plane for a 45° swept delta wing at $M_{\infty} = 3$ with inboard shock-induced separation, $R_{L_{\infty}} = 2.6 \times 10^6$ (Bluford, 1978).

1. Report No. NASA TM-81187		2. Government Accession No.		3. Recipient's Catalog No.	
4. Title and Subtitle LEEWARD FLOW OVER DELTA WINGS AT SUPERSONIC SPEEDS				5. Report Date	
				6. Performing Organization Code	
7. Author(s) Joachim G. Szodruch* and David J. Peake**				8. Performing Organization Report No. A-8117	
9. Performing Organization Name and Address Ames Research Center Moffett Field, Calif. 94035				10. Work Unit No. 506-51-11	
				11. Contract or Grant No.	
12. Sponsoring Agency Name and Address National Aeronautics and Space Administration Washington, D.C. 20546				13. Type of Report and Period Covered Technical Memorandum	
				14. Sponsoring Agency Code	
15. Supplementary Notes *National Research Associate **Consultant, 3-D Flowz, Inc.					
16. Abstract <p>A survey is made of the parameters affecting the development of the leeward symmetric separated flow over slender delta wings immersed in a supersonic stream. These parameters include Mach number, Reynolds number, angle of attack, leading-edge sweep angle, and body cross-sectional shape, such that subsonic and supersonic leading-edge flows are encountered. It is seen that the boundaries between the various flow regimes existing about the leeward surface may conveniently be represented on a diagram with the components of angle of attack and Mach number normal to the leading edge as governing parameters.</p> <p>Although the work in this field has been mainly experimental over the last twenty-five years, recent laminar-flow computations using approximate forms of the Navier-Stokes equations have provided details of the flow field that are in reasonable agreement with experimental results at low Reynolds numbers.</p>					
17. Key Words (Suggested by Author(s)) Delta wings Vortices Three-dimensional flow separation Shock boundary-layer interaction				18. Distribution Statement Unlimited STAR Category - 02	
19. Security Classif. (of this report) Unclassified		20. Security Classif. (of this page) Unclassified		21. No. of Pages 48	
				22. Price* \$4.50	

